ABSTRACT

Title of Thesis: NUMERICAL SIMULATION OF IGNITION AND TRANSIENT COMBUSTION IN FUEL VAPOR CLOUDS

Jennifer Wiley, Master of Science, 2007

Directed By: Professor Arnaud Trouvé
Department of Fire Protection Engineering

The Large-Eddy Simulation (LES) approach is used to model partially-premixed combustion (PPC) in confined and unconfined fuel vapor clouds. The model is based on the concept of a filtered reaction progress variable to describe the premixed combustion. The premixed combustion model is implemented into the Fire Dynamics Simulator (FDS), developed at the National Institute of Standards and Technology, USA, and is coupled with either an equilibrium-chemistry, mixture-fraction based model (FDS Version 4) or an eddy dissipation model (FDS Version 5) for non-premixed combustion. Modifications to the model are developed and implemented with the goal of reducing the grid resolution requirement while still producing physically sound results. The modified formulation is tested using both versions of the non-premixed combustion model, and the results are compared. It is found that the modifications are capable of reducing errors associated with poorly-resolved simulations in both versions of the model.

NUMERICAL SIMULATION OF IGNITION AND TRANSIENT COMBUSTION IN FUEL VAPOR CLOUDS

By

Jennifer Wiley

Thesis submitted to the Faculty of the Graduate School of the
University of Maryland, College Park, in partial fulfillment
of the requirements for the degree of
Master of Science
2007

Advisory Committee:

Professor Arnaud Trouvé, Chair
Professor André Marshall
Professor Gregory Jackson

Acknowledgements

This work could not have been completed without the assistance and support of many. I would first and foremost like to thank my advisor, Professor Arnaud Trouvé, for his support and guidance throughout the entire process. I would also like to thank the other members of my committee, Professor André Marshall and Professor Gregory Jackson, for their generous contribution of time and effort. This research is partially supported by the National Institute of Standards and Technology (NIST), and I would like to thank Dr. Kevin McGrattan at NIST for his support and guidance during this project and in the course of my growth and development in the field of fire modeling. I would also like to acknowledge the assistance of my colleague, Zhixin Hu (Sam), in helping me to understand the vagueries of computer code and for always being willing to be a sounding board for when I was experiencing difficulties with the model.

To the faculty and staff of the Fire Protection Engineering Department, I express my deepest gratitude for your kind guidance, support, and wisdom. You have made all of my years at the University of Maryland truly memorable. Finally, I must thank my parents and sisters for providing support, encouragement, and even comic relief when necessary. Thank you from the bottom of my heart.

Table of Contents

List of Figures

Chapter 1 Introduction

1.1 Overview

The occurrence of accidental fuel releases and their potential for deflagration or detonation if ignited has long been a problem of interest in the fire safety field. Experimental studies of these phenomena for real-scale scenarios, which may be on the order of tens of meters or greater, is cost-prohibitive. Therefore, there is a need to develop computational tools capable of handling the complex combustion problem presented by fuel vapor cloud ignition. The combustion dynamics of many accidental fuel release incidents require a model that allows combustion to occur as both premixed and non-premixed (diffusion), either simultaneously or sequentially. Combustion will be either premixed, non-premixed, or both depending on the fuel concentration in the cloud and on whether the fuel-air mixture is homogeneous. An example of one such partially-premixed combustion (PPC) sequence is presented in Figure 1.1. When fuel is released, it first mixes with the ambient air to form a cloud that may have regions that are flammable, ultra-rich, and ultra lean (Figure 1.1a), depending on the circumstances of the release. When an ignition source is introduced into the flammable region of the cloud (Figure 1.1b), a premixed flame is initiated and propagates to the edge of the flammable cloud (Figure 1.1c). If there exists an ultra-rich region in the cloud (usually near the fuel source), then "light-back" of the ultra-rich fuel may occur (Figure 1.1d) and the flame will transition to a diffusion flame anchored on the fuel source (Figure 1.1e).

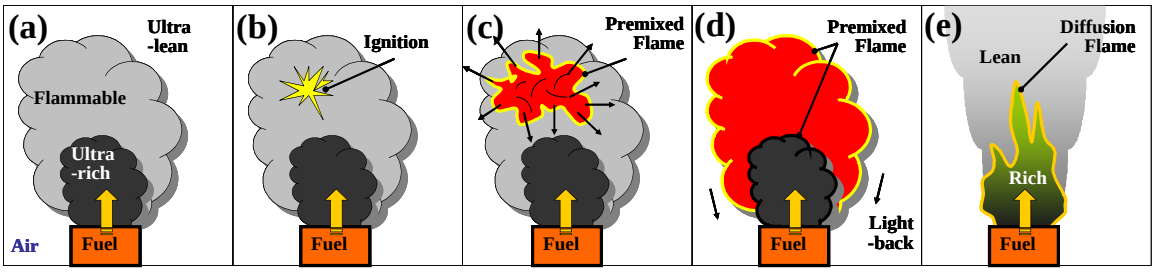

Figure 1.1: Example of a light back sequence: (a) fuel-air mixing; (b) ignition; (c) deflagration; (d) light-back; (e) transition to diffusion burning.

There is consequently a need to develop models that are capable of simulating partially-premixed combustion at a reasonable computational cost, so that large-scale problems of engineering interest may be studied cost-effectively. The Fire Dynamics Simulator (FDS), developed at the National Institute of Standards and Technology, USA, is widely used in the fire protection engineering field for simulations of non-premixed combustion and smoke movement [1, 2]. This model, however, does not currently incorporate a model for premixed combustion, and therefore neither premixed nor partially-premixed scenarios may be considered with the current solver. In the present work, we incorporate a premixed combustion model into the existing LES framework in the Fire Dynamics Simulator for non-premixed combustion, thereby enabling the study of partially-premixed combustion.

1.2 Literature Review

Accidental combustion of gaseous fuel clouds has long been a concern of the fire safety field. Previous CFD modeling efforts typically belong to one of the two following categories: studies in which flammable conditions are assumed across the bulk of the fuel vapor cloud, and combustion is premixed; and studies in which ultra-rich conditions are

assumed across the bulk of the fuel vapor cloud, and combustion is non-premixed. Only recently have researchers undertaken studies to couple the two combustion modes in order to develop models that allow both premixed and non-premixed combustion to occur, either simultaneously or sequentially, in what is known as partially-premixed combustion (PPC). This section will focus on previous modeling efforts, including CFD studies of premixed, non-premixed and partially-premixed combustion. Though many models and sub-models are required in order to develop a successful CFD package, the present discussion will be limited to those sub-models relevant to combustion.

Molkov and colleagues have developed and tested a model designed to simulate confined and unconfined gaseous deflagrations [3-5]. The model is based on a large-eddy simulation (LES) filtering of fully compressible conservation equations for mass, momentum, and energy, in addition to a reaction progress variable (RPV) *c*. The reaction progress variable is a non-conserved scalar quantity that takes values between zero and unity and separates the fresh reactants from the burnt products [6]. The gradient combustion method, in which the local mass burning rate is assumed to be proportional to the magnitude of the gradient of the reaction progress variable $|\nabla\tilde{c}|$ is used as a closure model for premixed combustion. A subgrid-scale (SGS) flame wrinkling factor (the ratio of the flame surface to its projection in the direction perpendicular to propagation [6], equal to 1 for a completely laminar flame) is also incorporated into the combustion model. The model is first developed for confined deflagrations and shown to produce results in agreement with theoretical and experimental results for deflagrations of a stoichiometric hydrogen-air mixture in a 2.3-m-diameter spherical vessel [3]. The model

is later adapted to the treatment of unconfined deflagrations, and the results of two different models for the turbulent burning velocity are compared to an experimental study of a near stoichiometric hydrogen-air deflagration in an unconfined hemispherical volume of diameter 20 m [4]. In order to adapt the model to the treatment of vented enclosures, the increase in flame front area due to disturbances from a vent opening is modeled by the use of a deflagration-outflow interaction (DOI) number, which takes into account venting parameters such a problem scale and the Bradley number, which incorporates vent size [5]. This model is then shown to produce good agreement with combustion experiments of fuel-lean to stoichiometric hydrogen-air mixtures conducted in vented enclosures of varying volumes, vent diameters, and vent-relief pressures.

Another effort to conduct large-eddy simulations of premixed combustion was undertaken by Knikker and coworkers [7]. This study also applies a reaction progress variable approach. However, the unresolved reaction rate is modeled using a flame surface density approach, in which the filtered fuel consumption rate is written as a product of a local laminar flame speed times a factor that corresponds to the flame surface area per unit volume, the flame surface density (FSD). This approach requires a model for both the resolved and unresolved FSD, and the authors select an algebraic form developed by Boger et al. [8] to describe the resolved FSD and a similarity concept is employed for the unresolved portion, wherein the unresolved FSD is assumed to be similar, in location and order of magnitude, to the contribution evaluated at the resolved scales. The model is tested against experimental data obtained by OH-radical laser-

induced fluorescence in a turbulent premixed propane-air flame, and is successful in reproducing the structure, location, and magnitude of the unresolved reaction rate.

A series of studies conducted by Makhviladze and coworkers provides an example of a model that assumes fuel rich conditions across the bulk of the flammable cloud and implements a non-premixed combustion model [9-12]. The model solves species equations for fuel, O2, N2, H2O, and CO2, along with an incompressible (low Mach number) form of the Navier-Stokes equations. An eddy break-up model is used for the reaction rate. In the eddy break-up model (EBU), the reaction zone is viewed as a collection of fresh and burnt gas pockets. The Kolmogorov cascade of turbulent kinetic energy suggests that turbulence leads to a breakdown in the structure of the fresh gases, and the reaction rate is therefore controlled by the turbulent mixing time [6]. The model is used to study the structure of the fireball resulting from the ignition of the vertical release of fuel from an axially-symmetric jet. Additionally, a comparison of model predictions to empirical relationships for fireballs provides reasonable results. A correlation for the fireball lifetime as a function of the Froude number is presented. Subsequent works [11, 12] extended the model to treatment of two-phase fuel releases (consistent with a liquefied fuel under pressure). Finally, the model was applied to simulate the development and combustion of a fuel vapor cloud formed from an instantaneous fuel release (in contrast with the finite-time releases of the previous studies) [13]. A correlation for the fireball lifetime is developed and compared with that previously determined for vertically directed fuel releases.

A widely-used model for simulation of non-premixed combustion is the Fire Dynamics Simulator, developed at the National Institute of Standards and Technology, USA [1, 2]. This model is developed for fire applications and thus uses an incompressible form of the Navier-Stokes equations, along with a mixture fraction model to describe local species concentrations. Depending on the version, FDS employs one of two different combustion sub-models. Version 4 of FDS uses a mixture fraction combustion model, while Version 5 uses an Eddy Dissipation (EDC) combustion model, similar to the previously described Eddy Break-up model. More details on each of these models are presented in Section 2.2. Because of its widespread use, the model has been extensively validated. More information on these validation efforts is available in Ref. [1].

Only recently have efforts been made to develop models capable of both premixed and non-premixed combustion modes in order to model partially-premixed combustion (PPC). These efforts are usually motivated by a need to adapt CFD models to the treatment of lifted diffusion flames; however the results may be applicable in any scenario in which the fuel and oxidizer are not completely premixed before combustion. Domingo et al. present one such effort in Ref. [14]. This paper explores the potential for using two separate models for premixed and non-premixed combustion along with a mechanism to couple the results of the two. The authors present the concept of a flame index in order to determine whether combustion is occurring locally as premixed or non-premixed, based on the product of the fuel and oxygen concentration gradients. When these gradients are parallel to each other, the fuel and oxygen are coming into the flame from the same direction, and the combustion is premixed. When they are perpendicular,

the fuel and oxygen enter the flame from opposite directions, and thus the combustion is non-premixed. The model predictions are then compared to experimental results of lifted diffusion flames, with promising results.

Müller and coworkers have developed a different method of addressing partially-premixed combustion [15]. Rather than employing a reaction progress variable c, the authors use a field equation for the scalar field G, whose level surface $G = G_0$ represents the premixed flame surface. This is combined with a mixture fraction Z, whose stoichiometric surface Z_{st} determines the location of the non-premixed flame. The resulting model is then used to predict flame propagation and liftoff in turbulent jet diffusion flames.

1.3 Objectives

The objective of this study is to develop a CFD model suitable for both research- and engineering-level treatments of partially-premixed combustion. Previous research efforts with this model [16-18] have demonstrated positive results for the model in a research-level framework (i.e. small-scale problems with finely meshed computational grids). Therefore, the focus of present work is to enhance the model so that reasonable results may be expected from the coarser grids and larger scale problems of interest to the fire safety engineer.

Chapter 2 Model Description

The partially-premixed combustion model is implemented into the Fire Dynamics Simulator (FDS), Version 4, CFD solver, developed at the National Institute of Standards and Technology, USA. This model is oriented towards fire applications and uses a Large Eddy Simulation (LES) approach for turbulence modeling and an equilibrium-chemistry, mixture-fraction-based model for non-premixed combustion [1, 19]. FDS does not currently have a premixed combustion capability in the publicly-released version. FDS solves a low-Mach number formulation of the Navier-Stokes equations, and therefore the PPC model is developed for deflagration scenarios, in which the premixed flame propagates at subsonic speeds and pressure remains quasi-uniform across the combustion zone. In anticipation of the upcoming release of Version 5 of FDS, the PPC model was also incorporated into this newer version of the solver [2]. The mixture-fraction combustion model of FDS Version 4 is compared to the eddy dissipation combustion model of FDS Version 5. These models are described in further detail in Section 2.2. This newest version of FDS incorporates optional models for local flame extinction and two-step combustion, but these models are not considered in the present work. It is left for future work to demonstrate the effectiveness of these models in the context of the PPC solver.

2.1 Deflagration Modeling

Here is presented the adaptation of the reaction progress variable method to describe premixed combustion. This particular model was first described in [18], the details of

which are repeated here. The deflagration model is based on the concept of a reaction progress variable *c*: $c = 0$ in the fresh reactants, $c = 1$ in the burnt products, and the flame is the region where *c* goes from 0 to 1 [6, 20, 21]:

$$c = \frac{(Y_F^m - Y_F)}{(Y_F^m - Y_F^{eq})} = \frac{(Y_{O_2}^m - Y_{O_2})}{(Y_{O_2}^m - Y_{O_2}^{eq})} = \frac{Y_{CO_2}}{Y_{CO_2}^{eq}} = \frac{Y_{H_2O}}{Y_{H_2O}^{eq}} \tag{2-1}$$

or equivalently:

$$\left.\begin{aligned} Y_F &= (1-c)\times Y_F^m + c \times Y_F^{eq} \\ Y_{O_2} &= (1-c)\times Y_{O_2}^m + c \times Y_{O_2}^{eq} \\ Y_{CO_2} &= c \times Y_{CO_2}^{eq} \\ Y_{H_2O} &= c \times Y_{H_2O}^{eq} \end{aligned}\right\} \tag{2-2}$$

where Y_k is the mass fraction of species *k*, Y_k^m the value of Y_k in the unburned gas, and Y_k^{eq} the value of Y_k in the burned gas. Y_k^m is an input quantity into the combustion problem that describes the pre-combustion state of the reactive mixture; whereas Y_k^{eq} describes the post-premixed combustion state of the mixture, and can be determined from equilibrium dynamics.

A transport equation based on a classical mass-balance equation is used for describing the *c*-field:

$$\frac{\partial}{\partial t}(\rho c)+\frac{\partial}{\partial x_i}(\rho u_i c)=\frac{\partial}{\partial x_i}\left(\rho D\frac{\partial c}{\partial x_i}\right)+\dot{\omega}_c \tag{2-3}$$

where ρ is the density, u_i is the x_i-component of the flow velocity vector, D the mass molecular diffusion coefficient, and $\dot{\omega}_c$ the reaction rate of c. To adapt this formulation to an LES framework, we first apply an LES filter to Eqn. (2-3):

$$\frac{\partial}{\partial t}\left(\overline{\rho}\widetilde{c}\right)+\frac{\partial}{\partial x_i}\left(\overline{\rho}\widetilde{u}_i\widetilde{c}\right)=-\frac{\partial}{\partial x_i}\left(\overline{\rho u_i c}-\overline{\rho}\widetilde{u}_i\widetilde{c}\right)+\frac{\partial}{\partial x_i}\left(\overline{\rho D\frac{\partial c}{\partial x_i}}\right)+\overline{\dot{\omega}_c} \tag{2-4}$$

where the over-bar denotes straight LES-filtered quantities while the tilde represents Favre-weighted (*i.e.* density-weighted) LES-filtered quantities. The first term on the right-hand side of Eqn. (2-4) represents convective transport of c due to subgrid-scale (SGS) turbulent fluctuations, while the second and third terms represent, respectively, the molecular diffusion of c and the production of c due to chemical reaction.

Closure models must now be adopted for the unknown terms on the right-hand side of Eqn. (2-5). For the SGS turbulent flux term, we choose to adopt a gradient transport model [6, 20]:

$$\left(\overline{\rho u_i c}-\overline{\rho}\widetilde{u}_i\widetilde{c}\right)=-\overline{\rho}\frac{\nu_t}{Sc_t}\frac{\partial\widetilde{c}}{\partial x_i} \tag{2-5}$$

where ν_t is the Smagorinsky turbulent eddy-diffusivity, and Sc_t is a turbulent Schmidt number.

For the reaction source term, we adopt a flamelet viewpoint in which it is assumed that the chemical reaction takes place in a thin propagating surface that locally resembles a laminar flame [22]. Further, we select a flame surface density approach, and write the volumetric chemical reaction rate as the product of a laminar-like reaction rate per unit flame surface area times a flame surface density [6, 20]:

$$\overline{\dot{\omega}}_c = \left(\rho_u s_L\right) \times \Sigma \tag{2-6}$$

where ρ_u is the density of the unburned gas, s_L is the laminar flame speed and Σ is the LES-filtered flame surface-to-volume ratio. Here, we use an algebraic expression for Σ, proposed by Veynante and co-workers [8, 23-25]:

$$\Sigma = \Xi \times 4\sqrt{\frac{6}{\pi}}\frac{\widetilde{c}(1-\widetilde{c})}{\Delta_c} \tag{2-7}$$

where Ξ is the SGS flame wrinkling factor and Δ_c is the LES filter size for the *c*-equation. In the following, we neglect subgrid-scale wrinkling and assume $\Xi = 1$.

Finally, we adopt the closure model of Ref. [25], based on the Kolmogorov-Petrovskii-Piskunov (KPP) theory, to describe the molecular diffusion transport of *c*:

$$\overline{\rho D \frac{\partial c}{\partial x_i}} = \frac{\rho_u s_L \Delta_c}{16\sqrt{6/\pi}} \frac{\partial \widetilde{c}}{\partial x_i} \tag{2-8}$$

Equations (2-4)-(2-8) can then be combined to write the final form of the transport equation for the reaction progress variable:

$$\frac{\partial}{\partial t}(\overline{\rho}\widetilde{c}) + \frac{\partial}{\partial x_i}(\overline{\rho}\widetilde{u}_i\widetilde{c}) = \frac{\partial}{\partial x_i}((\overline{\rho}\frac{\nu_t}{Sc_t} + \frac{\rho_u s_L \Delta_c}{16\sqrt{6/\pi}})\frac{\partial \widetilde{c}}{\partial x_i}) + 4\rho_u s_L \Xi \sqrt{\frac{6}{\pi}} \frac{\widetilde{c}(1-\widetilde{c})}{\Delta_c} + \overline{\dot{\omega}}_{ign} \tag{2-9}$$

where $\overline{\dot{\omega}}_{ign}$ is an extra ignition source term used as a numerical spark to initiate premixed combustion.

The corresponding LES-filtered premixed heat release rate (HRR) per unit volume is:

$$\overline{\dot{q}}_p''' = (\overline{\dot{\omega}}_c + \overline{\dot{\omega}}_{ign}) \times (Y_F^m - Y_F^{eq}) \Delta H_F = (4\rho_u s_L \Xi \sqrt{\frac{6}{\pi}} \frac{\widetilde{c}(1-\widetilde{c})}{\Delta_c} + \overline{\dot{\omega}}_{ign}) \times (Y_F^m - Y_F^{eq}) \Delta H_F \tag{2-10}$$

Previous work [17] has determined the grid resolution requirement for the premixed combustion model. In order to properly resolve the flame, the grid resolution must be considerably finer than that required to resolve the turbulent flow. This increase in resolution is often computationally cost-prohibitive. Therefore the authors suggest that the LES *c*-filter size Δ_c be increased to a value greater than the computational grid size Δ, so that the grid may be designed to the less-demanding standard of the turbulence model.

Therefore the filter-to-grid length scale ratio Δ_c/Δ is treated here as a model parameter. The authors then proceed to evaluate the effect of the filter-to-grid length scale ratio on the quality of the simulation, and recommend that $\Delta_c/\Delta \geq 5$ is sufficient to resolve the flame. Consequently, $\Delta_c = 5\Delta$ is used in the following simulations.

2.2 Diffusion Flame Modeling

The diffusion flame model implemented in the Fire Dynamics Simulator, developed by the National Institute of Standards and Technology, USA is retained here. Because this paper presents work from both Version 4 and Version 5 of FDS, both models are described below.

2.2.1 Fire Dynamics Simulator, Version 4

The non-premixed combustion model in Version 4 of FDS is based on the classical Burke-Schumann theory of diffusion flames in which infinitely fast chemistry is assumed and the flame structure is described in terms of a conserved mixture fraction $\widetilde{Z}$. In most fire situations, the turbulent motions are buoyancy driven and the turbulence intensities remain low-to-moderate. Under such conditions with well-ventilated environments, flame extinction is unlikely, and the assumption of infinitely fast chemistry is reasonable. As shown in Ref. [26], the Burke-Schumann theory also produces explicit expressions for the chemical reaction rates. The LES-filtered (non-premixed) fuel mass reaction rate may be written as:

$$\overline{\dot{\omega}}_F = -\left(\frac{Y_F^{\infty}}{1-Z_{st}}\right)\left(\frac{1}{2}\overline{\rho}\widetilde{\chi}_{st}\right)\widetilde{p}(Z_{st}) \qquad (2\text{-}11)$$

where Y_F^{∞} is the fuel mass fraction in the fuel supply stream (usually assumed to be 1), $\widetilde{\chi}_{st}$ the LES-filtered value of scalar dissipation rate (averaged along the subgrid-scale flame surface contour $Z = Z_{st}$), and where $\widetilde{p}(Z_{st})$ is the stoichiometric value of the (Favre-weighted) probability density function (Pdf) that describes subgrid-scale variations in Z.

We now introduce additional simplifications for the description of the conditional mixing rate $\widetilde{\chi}_{st}$ and the Pdf value $\widetilde{p}(Z_{st})$. First, we assume that $\widetilde{\chi}_{st}$ may be approximated by the unconditional scalar dissipation rate $\widetilde{\chi}$; we write [27]: $\widetilde{\chi} \approx 2(\nu_t / Sc_t)\left|\nabla\widetilde{Z}\right|^2$. Second, we assume that $\widetilde{p}(Z_{st})$ may be approximated using a δ-Pdf closure expression: $\widetilde{p}(Z_{st}) = \delta(\widetilde{Z} - Z_{st})$. The δ-Pdf approximation is a crude presumed Pdf model in which subgrid-scale variations in Z are simply neglected. While clearly questionable, this closure model is adopted here because it complies with the simple realizability requirement that under well-ventilated conditions, all the fuel mass coming from the fuel source is actually consumed by the turbulent flame [28]. As shown in Ref. [28], more elaborate presumed Pdf expressions do not necessarily satisfy this realizability requirement and therefore fail to predict the correct global HRR.

The corresponding expression for the LES-filtered HRR per unit volume is:

$$\bar{q}_d''' = \left(\frac{Y_F^\infty}{1 - Z_{st}}\right)\left(\bar{\rho}\,\frac{\nu_t}{Sc_t}\left|\nabla \tilde{Z}\right|^2\right)\delta(\tilde{Z} - Z_{st}) \times \Delta H_F \tag{2-12}$$

Equation (2-12) is currently implemented into the Fire Dynamics Simulator, Version 4 [1, 19].

2.2.2 Fire Dynamics Simulator, Version 5

We now turn to the description of the combustion model in Version 5 of FDS, which incorporates significant changes to the mixture fraction and combustion models. We first describe the new mixture fraction formulation. The mixture fraction is defined in terms of the mass fractions of fuel (C_xH_y) and the products of combustion containing carbon [2]:

$$Z = Y_F + \frac{W_F}{xW_{CO_2}} Y_{CO_2} + \frac{W_F}{xW_{CO}} Y_{CO} + \frac{W_F}{xW_C} Y_C \tag{2-13}$$

where W_k is the molecular weight of species k. This mixture fraction is then separated into two components:

$$Z_1 = Y_F$$

$$Z_2 = \frac{W_F}{xW_{CO_2}} Y_{CO_2} + \frac{W_F}{xW_{CO}} Y_{CO} + \frac{W_F}{xW_C} Y_C \tag{2-14}$$

$$Z = Z_1 + Z_2$$

A transport equation must be solved for each of these mixture fractions. However, this formulation has the benefit of allowing inert mixing of reactants to occur. In this way, the mixture fraction Z_1 describes the state of the mixture if only mixing is occurring with no combustion, while the mixture fraction Z_2 describes the state of the mixture after the reaction has been completed [2]. This latter set of state relations corresponds to the classical Burke-Schumann equilibrium solution. If Y_k^m represents the species fuel mass fraction in the pure mixing solution, and Y_k^{eq} represents the equilibrium solution (see Figure 2.1), then the local mass fraction may be written as a linear combination of these two solutions:

$$Y_k = \left(1 - c^*\right) \times Y_k^m + c^* \times Y_k^{eq} \tag{2-15}$$

where c^* is a reaction progress variable to describe the state of the non-premixed combustion. Unlike the reaction progress variable for premixed combustion introduced in Section 2.1, this progress variable is calculated locally from the values of the LES-filtered mixture fractions $\widetilde{Z}_1$ and $\widetilde{Z}_2$ and is not transported [2]:

$$c^* = \frac{\widetilde{Z} - \widetilde{Z}_1}{\widetilde{Z} - Y_F^{eq}\left(\widetilde{Z}\right)} = \frac{\widetilde{Z}_2}{\widetilde{Z} - Y_F^{eq}\left(\widetilde{Z}\right)} \tag{2-16}$$

This progress variable c^* has similar features to the premixed reaction progress variable $\widetilde{c}$. When $\widetilde{Z}_2 = 0$, there are no products and therefore $c^* = 0$ and the mixture corresponds to pure reactants, whereas when $\widetilde{Z}_1 = Y_F^{eq}\left(\widetilde{Z}\right)$, then $c^* = 1$ and the mixture is at its post-combustion state.

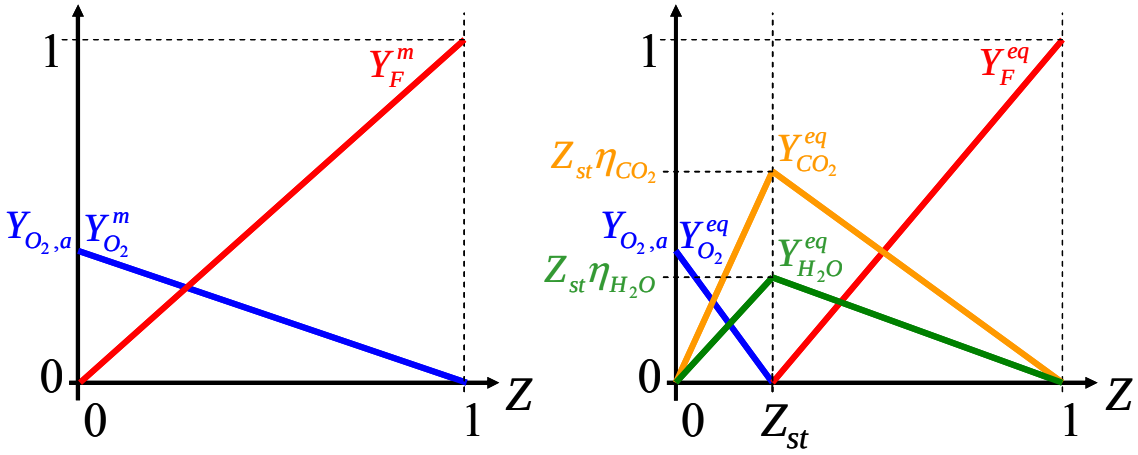

Figure 2.1: State relations for pure mixing of reactants (left) and post-combustion, equibrium state (right).

The chemical mass reaction rate is then calculated using an eddy dissipation combustion model [29]:

$$\overline{\dot{\omega}}_F = \frac{\overline{\rho}}{\delta t} \times \min\left(\widetilde{Y}_F, \frac{\widetilde{Y}_{O_2}}{r_s}\right) \tag{2-17}$$

where δt is the time step and r_s is the stoichiometric oxygen-to-fuel mass ratio. Note that unlike the combustion model of FDS4, this formulation allows for combustion to occur anywhere fuel and oxygen coexist, rather than limiting combustion to the vicinity of the stoichiometric iso-contour. Though FDS incorporates a model to determine local flame extinction, this model is not considered in the present study and therefore will not be presented here. The corresponding heat release rate per unit volume is:

$$\overline{\dot{q}}_d''' = \overline{\dot{\omega}}_F \Delta H_F = \frac{\overline{\rho} \Delta H_F}{\delta t} \times \min\left(\widetilde{Y}_F, \frac{\widetilde{Y}_{O_2}}{r_s} \right) \tag{2-18}$$

Finally, the mixture fractions $\widetilde{Z}_1$ and $\widetilde{Z}_2$ are updated [2]:

$$\widetilde{Z}_1(t+\delta t) = \widetilde{Z}_1(t) - \frac{\overline{\dot{\omega}}_F \cdot \delta t}{\overline{\rho}}; \quad \widetilde{Z}_2(t+\delta t) = \widetilde{Z}_2(t) + \frac{\overline{\dot{\omega}}_F \cdot \delta t}{\overline{\rho}} \tag{2-19}$$

while the total mixture fraction (and by extension the fuel mass) $Z = Z_1 + Z_2$ remains conserved.

2.3 Partially-Premixed Combustion Modeling

In order to treat partially-premixed (PPC) combustion scenarios, the deflagration model must first be adapted to include non-homogenous distributions of the mixture fraction. For non-homogeneous mixtures, both Y_k^m and Y_k^{eq} are functions of the local mixture

fraction $\widetilde{Z}$, as described in Figure 2.1 above. For $\widetilde{c}$ = 0, the mixture consists of unburned reactants, and corresponds to the pure mixing solution, Y_k^m. For $\widetilde{c}$ = 1, premixed combustion is complete, and the mixture composition corresponds to the Burke-Schumann solution, Y_k^{eq}. The state relationships can then be written as a weighted average between the pure mixing and equilibrium solutions, with $\widetilde{c}$ as a weight coefficient:

$$Y_k = (1-\widetilde{c}) \times Y_k^m + \widetilde{c} \times Y_k^{eq} \tag{2-20}$$

Note that this is similar to the expression presented in Eqn. (2-15), with the exception that here we are using the premixed reaction progress variable $\widetilde{c}$ instead of the more general c^*. In fact, the PPC model implemented into FDS Version 5 uses the state relations expressed in Eqn. (2-15), with the exception that the fuel source term in the $\widetilde{Z}_1$ and $\widetilde{Z}_2$ equations, the values of which are used to calculate c^*, is defined as follows:

$$\begin{gathered}\overline{\dot{\omega}}_F^* = FI \times \overline{\dot{\omega}}_c (Y_F^m - Y_F^{eq}) + (1-FI) \times f_{ign} \times \overline{\dot{\omega}}_F \\ \widetilde{Z}_1(t+\delta t) = \widetilde{Z}_1(t) - \frac{\overline{\dot{\omega}}_F^* \cdot \delta t}{\overline{\rho}}; \quad \widetilde{Z}_2(t+\delta t) = \widetilde{Z}_2(t) + \frac{\overline{\dot{\omega}}_F^* \cdot \delta t}{\overline{\rho}}\end{gathered} \tag{2-21}$$

where the flame index *FI* is used to determine whether the local mode of combustion is premixed or non-premixed and is described below, and f_{ign} is an *ad hoc* ignition factor. f_{ign} is introduced in Eqn. (2-21) so that the diffusion flame model remains inactive when

inert mixing is taking place ($f_{ign} = 0$ when $\widetilde{c} = 0$), and is only activated as a post-premixed-flame event ($f_{ign} = 1$ when $\widetilde{c} = 1$). In the following, we use the expression

$$f_{ign} = 0.5 + 0.5\tanh((\widetilde{c} - 0.6)/0.05) \tag{2-22}$$

unless otherwise noted.

The local laminar flame speed s_L must also be revised to allow varying mixture fractions. We propose to describe s_L through an *ad-hoc* analytical expression parametrized in terms of four input variables, called Z_{LFL}, Z_{UFL}, Z_{st} and $s_{L,st}$. Z_{LFL} and Z_{UFL} are the values of Z at the lower and upper flammability limits; Z_{st} and $s_{L,st}$ are the stoichiometric values of Z and s_L. We use here a presumed polynomial function that vanishes at Z_{LFL} and Z_{UFL}, is maximum at Z_{st}, and features a peak value equal to $s_{L,st}$ (Figure 2.2).

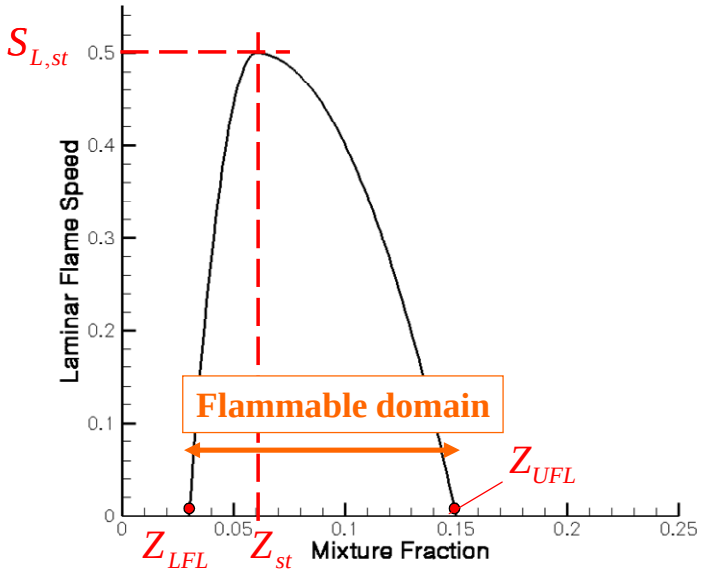

Figure 2.2: Variations of the laminar flame speed s_L with the mixture fraction.

Finally, in order to determine the total volumetric heat release rate $\bar{\dot{q}}'''$, a method must be developed for determining the local mode of combustion, whether premixed, or non-premixed. We use here the concept of an LES-resolved flame index *FI*. Following Ref. [14], we define the flame index as:

$$FI = \frac{1}{2}\left(\frac{\nabla \widetilde{Y}_F . \nabla \widetilde{Y}_{O_2}}{\left|\nabla \widetilde{Y}_F\right| \times \left|\nabla \widetilde{Y}_{O_2}\right|} + 1\right) \tag{2-23}$$

where $\widetilde{Y}_F$ and $\widetilde{Y}_{O_2}$ are given by Eqn. (2-20) in the context of FDS4 and Eqn. (2-15) in FDS5. Note that this expression differs slightly from that in Ref. [14]: the *FI*-expression in Ref. [14] includes a subgrid-scale contribution, which has been neglected in Eqn. (2-23).

Finally, the total local volumetric heat release rate may be written:

$$\bar{\dot{q}}''' = FI \times \bar{\dot{q}}_p''' + (1 - FI) \times f_{ign} \times \bar{\dot{q}}_d''' \tag{2-24}$$

where $\bar{\dot{q}}_p'''$ is as defined in (2-10), and $\bar{\dot{q}}_d'''$ is as defined in equations (2-12) and (2-18) for version 4 and 5 of FDS, respectively.

The grid resolution requirement of the PPC model is evaluated in terms of the gradient thickness of the mixture fraction distribution L_z in the context of Version 4 of FDS in Ref. [16]. The characteristic length scale L_z is defined as the total variation of the mixture fraction $\widetilde{Z}$ (assumed here to be between 0 and 1) divided by the maximum gradient of $\widetilde{Z}$. It is found that a length scale ratio of $\Delta_c/L_z \leq 1/8$ is required to provide a correct transition from premixed to diffusion burning in the case of a simplified flame propagation configuration. Recalling that we have selected $\Delta_c = 5\Delta$, this grid resolution requirement may be rewritten $L_z/\Delta \geq 40$. This is compared to typical grid resolution requirements for turbulent mixing or turbulent diffusion flame problems of $L_z/\Delta \geq 10$ - 20. Thus, the three-dimensional computational grid size required by the PPC formulation is approximately one to two orders of magnitude larger than usual. This requirement may be cost-prohibitive for current practical LES simulations: this problem is addressed in subsequent chapters.

Chapter 3 Unconfined Configuration

The ability of the model to accurately simulate both the transient and steady state features of a lifted partially-premixed flame was next tested. A lifted partially-premixed flame occurs when pure fuel or a fuel/oxidizer mixture is leaked or injected into an oxidizer at high velocities at concentrations greater than stoichiometric (Figure 3.1). Near the burner, fuel mixes inertly with the ambient oxidizer before reaching a premixed flame zone. If the fuel concentration is fuel-rich flammable, the fuel/oxidizer mixture will then burn in the premixed mode until all of the available oxygen is consumed. After premixed combustion has occurred, excess fuel and products of combustion are convected away from the premixed flame. These gases diffuse into the surrounding oxidizer and as a result, a diffusion flame forms at the edge of the product plume.

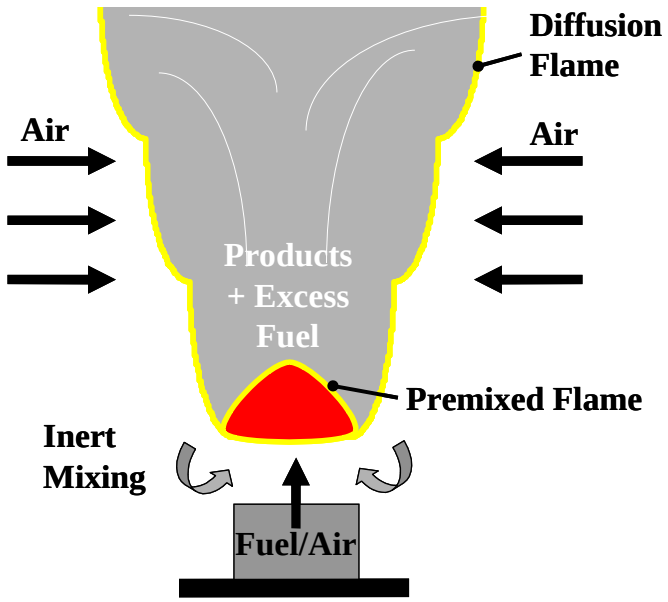

Figure 3.1: Representation of a lifted partially-premixed flame.

The model was implemented into FDS, Version 4, and tested in an unconfined partially-premixed combustion scenario. For this scenario, an open computational domain of size 1.44 m x 1.44 m x 1.0 m in height was used. A uniform grid size of 0.02 m on a side was used for a total grid of $72 \cdot 72 \cdot 50 = 259{,}200$ cells. A propane-air mixture ($Z = 0.12$) was supplied at a velocity of 0.35 m/s from a square burner of dimension 0.2 m centered at the base of the domain. The fuel-rich flammable source mixture fraction of 0.12 was selected so that the resulting combustion would be partially premixed. The maximum steady state heat release rate is therefore:

$$\begin{aligned} \dot{Q} &= \rho_u u_0 A Y_{f,0} \Delta H_F \\ &= 1.25\,kg/m^3 \cdot 0.35\,m/s \cdot 0.04\,m^2 \cdot 0.12 \cdot 47{,}251\,kJ/kg = 99\,kW \end{aligned} \tag{3-1}$$

where ρ_u is the density of the unburned fuel/air mixture, u_0 is the fuel/air supply velocity, A is the area of the burner, $Y_{f,0}$ is the mass fraction of fuel in the burner fuel jet, and ΔH_c is the heat of combustion of propane. This assumes that all fuel is combusted within the computational domain, which is not guaranteed due to the unconfined nature of the experiment. The heat release rate in the initial transient stage of combustion may be higher than this value, as the flame consumes the fuel that has already accumulated in the compartment. The laminar flame speed of the propane was 0.5 m/s. The stoichiometric mixture fraction is 0.062, while the upper and lower flammable mixture fractions are 0.03 and 0.15, respectively. For this test case, gravitational effects were not considered, and a co-flow of air at 0.4 m/s was applied surrounding the fuel source to prevent excess expansion of the fuel stream. The mixture was ignited at a height of 0.5

m, in a location near the edge of the fuel plume (Figure 3.2). A plume of fuel gases was allowed to develop before ignition, so that the propagation of the flame back towards the source could be observed.

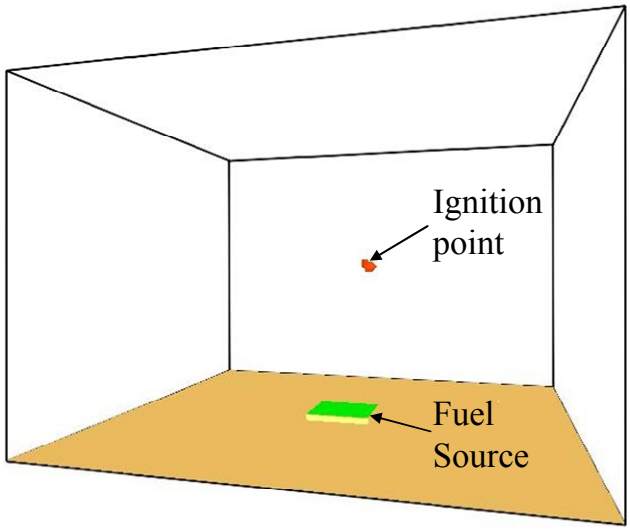

Figure 3.2: Validation test configuration.

3.1 Model Results

The results of the open configuration, in terms of the heat release rates, are shown in Figure 3.3. As expected, the premixed heat release rate increases rapidly to form a peak just after ignition. This peak corresponds to a deflagration through the fuel gases already present in the domain at the time of ignition. The diffusion flame lags slightly behind the premixed flame and is of lower intensity, as less fuel is available to burn in diffusion mode in the wake of the premixed flame. Both flames propagate back towards the source until they become stabilized above it, thereby initiating a quasi-steady period. The total steady state heat release rate is somewhat lower than the anticipated maximum of 99 *kW*,

indicating that a considerable amount of fuel is escaping through the upper boundary of the computational domain.

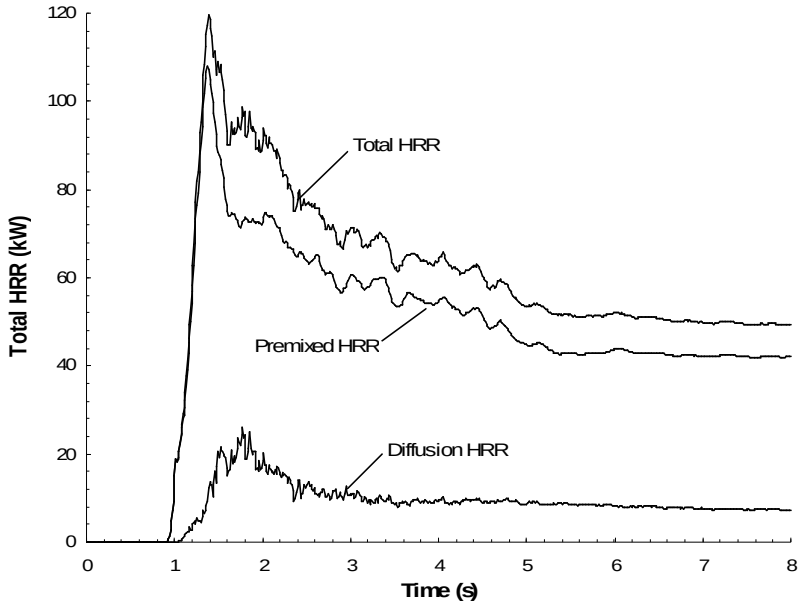

Figure 3.3: Total heat release rates for the open compartment configuration.

Visual evidence of the flame behavior in the steady state period is presented in Figure 3.4. A strong premixed flame has been established above the fuel source. Meanwhile, a diffusion flame is developed along the edges of the fuel plume to burn the fuel not initially consumed by the diffusion flame. This double flame structure has been documented in previous studies [30-35]. Note that the premixed flame also exhibits burning along the edge of the plume. This burning is not physical, as only diffusion burning should take place at the plume edges. This is also evident in the heat release rates in the upper portion of the domain (Figure 3.5):

$$\int_{x\min}^{x\max}\int_{y\min}^{y\max}\int_{0.5z\max}^{z\max} FI \times \bar{q}_p'''dxdydz \tag{3-2}$$

where it is expected that the premixed heat release rate should go to zero after the initial transient stage. In this case, a residual premixed heat release rate is still maintained in the steady state period. A more in-depth examination of the model results and a proposed solution to this error are presented in the following section.

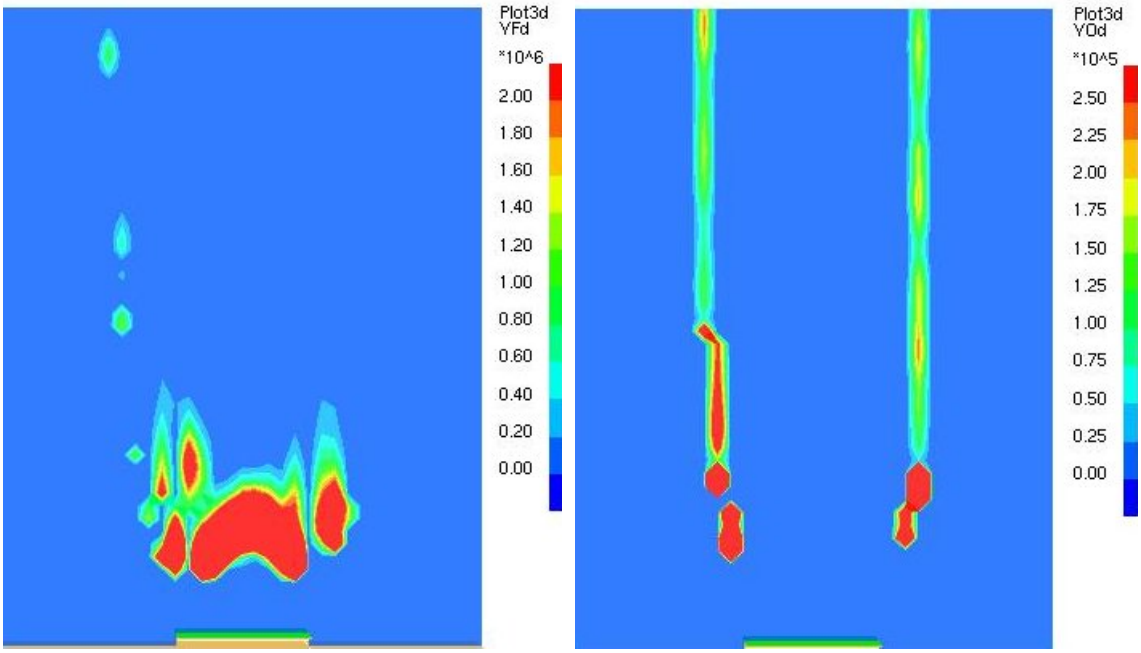

Figure 3.4: Distribution of the premixed heat release rate (left) and diffusion heat release rate (right) for the open compartment configuration (W/m^3).

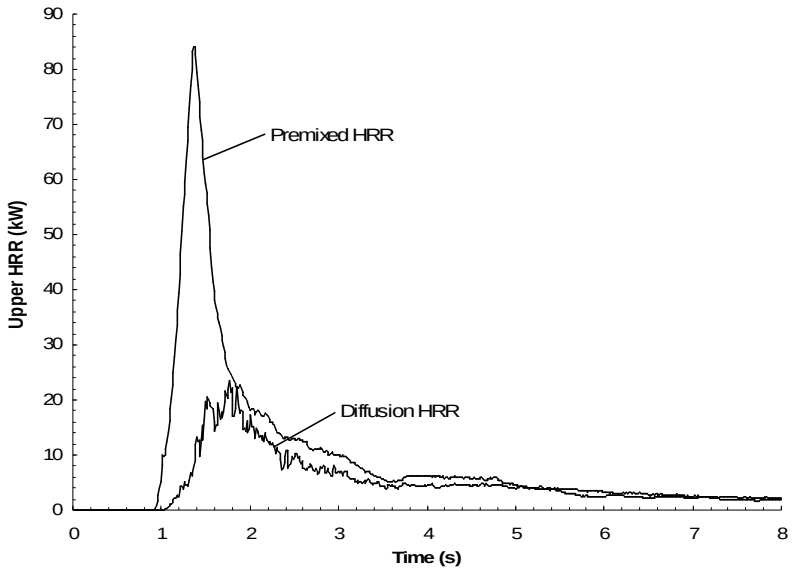

Figure 3.5: Heat release rates for the open compartment configuration in the upper half of the domain.

3.2 Improvements to the Premixed Combustion Model

In the interest of creating a model of practical engineering use, it was necessary to address errors in the model that arise as a result of using coarse grid scales. The reaction progress variable may be said to be thick on the grid. In other words, the variation of the progress variable from zero to one takes place over several grid cells. This variation of the progress variable occurs both where premixed burning is taking place (production of the progress variable) as well as where burnt gases ($\widetilde{c} = 1$) come in contact with unburnt gases ($\widetilde{c} = 0$). This highlights the dual nature of the reaction progress variable. Where the mixture composition is flammable, the reaction progress variable represents the progress of the premixed combustion reaction. However, where the mixture composition is not flammable, the progress variable becomes a mixing variable between products of combustion and unburnt reactants, or the ambient environment. This mixing, in combination with the necessity that the progress variable must be thick on the grid, leads

to erroneous premixed combustion at the edges of the flammable cloud for poorly-resolved $\widetilde{c}$ -fields. Near the edges of the product cloud, intermediate values of the progress variable may coincide with flammable values of the mixture fraction, thus allowing for premixed combustion to occur (Figure 3.6). When the grid is fine, the mixture fraction will not vary as much over the flame thickness, so that even when the $\widetilde{c}$ -field is not perfectly sharp, the mixture fraction will still be close to the lower flammable limit at the edge of the flame, meaning in turn that the flame speed will be close to zero. When the grid is coarse, the mixture fraction may vary greatly over the flame thickness, meaning that both flammable values of the mixture fraction and intermediate values of $\widetilde{c}$ coexist, causing errors. Due to the high resolution requirements of the $\widetilde{c}$ -field, as established by Williamson, McGill, and Trouvé [17], in most cases of engineering interest it is not practical to implement the grid requirements that would allow for a sufficiently high resolution of the progress variable. Thus efforts were made to modify the premixed combustion model in order to reduce these errors while also keeping the computational cost at a reasonable level.

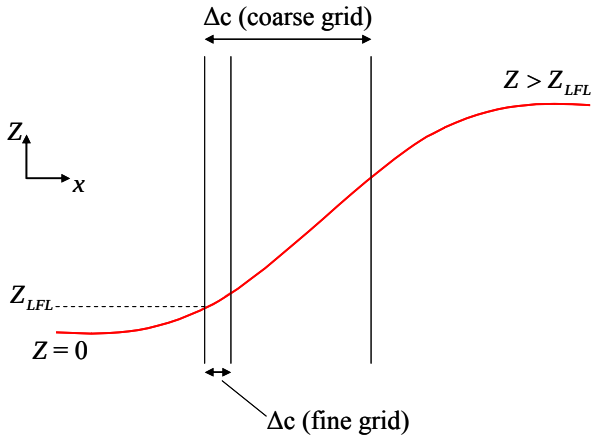

Figure 3.6: Effect of grid size on plume edge errors.

In order to validate changes to the algorithm, the model was tested again in the unconfined partially-premixed combustion scenario described previously. The goal of the present study was to eliminate or minimize premixed combustion that occurred along the edges of the fuel plume, where only diffusion burning is expected. To this end, each heat release rate component was integrated over the upper half of the computational domain, where it was assumed that any premixed burning would be along the edges of the plume and therefore erroneous. The percent error was then calculated as the percentage of the total heat release rate in this upper portion that was attributable to premixed combustion:

$$\%\ error = \frac{\int_{x\min}^{x\max}\int_{y\min}^{y\max}\int_{0.5z\max}^{z\max} FI \times \dot{\bar{q}}_p'''\, dxdydz}{\int_{x\min}^{x\max}\int_{y\min}^{y\max}\int_{0.5z\max}^{z\max} \dot{\bar{q}}'''\, dxdydz} \tag{3-3}$$

Modification of the calculation of the laminar flame speed s_L was identified as a potential method of reducing the premixed combustion error. One such modification involved replacing the local laminar flame speed with a spatially averaged flame speed $\bar{s}_L$, with flame speeds towards the edge of the flammable cloud ($\tilde{c} = 0$) given more weight:

$$\bar{s}_L(x,y,z) = \frac{\int_{x-2\Delta}^{x+2\Delta}\int_{y-2\Delta}^{y+2\Delta}\int_{z-2\Delta}^{z+2\Delta} s_L(x,y,z) * e^{-4\tilde{c}}\, dzdydx}{\int_{x-2\Delta}^{x+2\Delta}\int_{y-2\Delta}^{y+2\Delta}\int_{z-2\Delta}^{z+2\Delta} e^{-4\tilde{c}}\, dzdydx} \tag{3-4}$$

Although this modification was only applied for values of the mixture fraction near the lower flammability limit, it was ultimately unsuccessful due to the dependence of the reaction progress variable on the flame speed. By reducing the value of the flame speed near the edges of the flammable cloud, the propagation of the flame (through the RPV) was hindered as well.

In limiting premixed errors on the edges of the cloud, there are two goals. First we want to take the value of the premixed heat release rate to zero at the edge of the flammable cloud, which would call for low values of the laminar flame speed. At the same time, we want to maintain good propagation characteristics so that the reaction progress variable is equal to one over the entire flammable cloud. This would require higher values of the flame speed. These two (apparently contradictory) goals would suggest that two values of the laminar flame speed be calculated. One flame speed, designed to be small, would be used in the calculation of the premixed heat release rate, while the other, designed to be large, would be used in the reaction progress variable equation.

Models for these new flame speeds were developed, and a method was developed to locate the edges of the flammable cloud and to apply the modified flame speeds to those regions only. First, a search of the grid cells surrounding the cell of interest produced the minimum and maximum mixture fraction within a radius of 2 grid cells. If

$$Z_{\min} < Z_{LFL} \text{ and } Z_{\max} > Z_{LFL}$$
$$\textit{or if } Z_{\min} < Z_{UFL} \text{ and } Z_{\max} > Z_{UFL} \tag{3-5}$$

the cell is considered to be on an edge and the following modified flame speeds are applied:

$$\bar{s}_L(x,y,z) = \frac{\int_{x-2\Delta}^{x+2\Delta}\int_{y-2\Delta}^{y+2\Delta}\int_{z-2\Delta}^{z+2\Delta} s_L(x,y,z) * e^{-4\tilde{c}}\, dzdydx}{\int_{x-2\Delta}^{x+2\Delta}\int_{y-2\Delta}^{y+2\Delta}\int_{z-2\Delta}^{z+2\Delta} e^{-4\tilde{c}}\, dzdydx} \tag{3-6}$$

$$\bar{s}_{L,M}(x,y,z) = \frac{\int_{x-2\Delta}^{x+2\Delta}\int_{y-2\Delta}^{y+2\Delta}\int_{z-2\Delta}^{z+2\Delta} s_L(x,y,z) * e^{-4(1-\tilde{c})}\, dzdydx}{\int_{x-2\Delta}^{x+2\Delta}\int_{y-2\Delta}^{y+2\Delta}\int_{z-2\Delta}^{z+2\Delta} e^{-4(1-\tilde{c})}\, dzdydx} \tag{3-7}$$

where $\bar{s}_L$ is used in the calculation of the heat release rate (Eqn. (2-10)), and $\bar{s}_{L,M}$ is used in the transport equation for the reaction progress variable (Eqn. (2-9)). Where the edge conditions do not apply, the local value of the laminar flame speed $s_L(x,y,z)$ is applied without modification.

While this method produced positive results, the computational costs were high, reaching a maximum of almost five times the cost of an unmodified version of the PPC solver. Though various techniques were applied to reduce the execution time of the model, none were successful in bringing the computational costs down to an acceptable level. Additionally, these methods significantly reduced the magnitude of the initial transient peak in the premixed reaction rate. Ideally, any proposed modification would have the effect of taking the premixed heat release rate to zero in the quasi-steady state period while leaving the transient peak unchanged.

The high cost of the previous method was due both to the search necessary to identify $Z_{\min}$ and $Z_{\max}$ as well as the high cost of performing four triple integrations. The next modification involved estimating $Z_{\min}$ and $Z_{\max}$ by use of a local gradient. $\bar{s}_L$ and $\bar{s}_{L,M}$ were then calculated using a more brute force approach that involved using the appropriate minimum or maximum mixture fraction as the local mixture fraction. The quantity

$$\left(Z_{\min} - Z_{LFL}\right)\cdot\left(Z_{\max} - Z_{LFL}\right) \tag{3-8}$$

was used to identify whether a given edge cell was located along the lean edge $\left(Z_{\min} < Z_{LFL} < Z_{\max}\right)$ or along the rich edge $\left(Z_{\min} < Z_{UFL} < Z_{\max}\right)$. This quantity is negative for the lean edge condition and positive for the rich edge condition. $\bar{s}_L$ was then calculated using the value of $Z_{\min}$ or $Z_{\max}$ that would minimize the value of $\bar{s}_L$. Similarly, values of the mixture fraction were chosen to maximize $\bar{s}_{L,M}$. That is, for the lean edge condition,

$$\bar{s}_L = s_L\left(Z_{\min}\right) \text{ and } \bar{s}_{L,M} = s_L\left(Z_{\max}\right) \tag{3-9}$$

and for the rich edge condition:

$$\bar{s}_L = s_L\left(Z_{\max}\right) \text{ and } \bar{s}_{L,M} = s_L\left(Z_{\min}\right) \tag{3-10}$$

By definition, $Z_{\min} < Z_{LFL}$ for the lean edge and $Z_{\max} > Z_{UFL}$ for the rich edge. Thus the effect of the new method is to force $\bar{s}_L = 0$. Although this method significantly reduced the calculation costs, the results were noisy and inconsistent with the findings from the unmodified case (even with allowance for improvement). This method also resulted in a premixed heat release rate that was much lower in the transient propagation period of the calculation.

The best method, in terms of both cost-effectiveness and quality of results, was the result of combining the better results of the search method for $Z_{\min}$ and $Z_{\max}$ with the faster brute force method of calculating $\bar{s}_L$ and $\bar{s}_{L,M}$. An improved method for detecting edge conditions was applied to eliminate the possibility that regions where $Z_{\min} < Z_{LFL} < Z_{UFL} < Z_{\max}$ would be treated as edge conditions. The quantity

$$\left(Z_{\min} - Z_{LFL}\right)\cdot\left(Z_{\max} - Z_{LFL}\right)\cdot\left(Z_{\min} - Z_{UFL}\right)\cdot\left(Z_{\max} - Z_{UFL}\right) \tag{3-11}$$

is less than zero for edge conditions and greater than zero at non-edges or where the variation of Z is large enough that the search area exceeds the range of Z described above. This model retains the method of discriminating between edges on the fuel lean side of the cloud and edges on the fuel rich side of the cloud and applying the values of $Z_{\min}$ and $Z_{\max}$ accordingly so that $\bar{s}_{L,M}$ is maximized. Furthermore, $\bar{s}_{L,M}$ is set to be the

maximum of the result calculated with the new method or the unmodified local flame speed:

$$\bar{s}_{L,M}(x,y,z) = \max\left(\bar{s}_{L,M}(x,y,z),\ s_L(x,y,z)\right) \tag{3-12}$$

to ensure that the modification does not have the effect of reducing $\bar{s}_{L,M}$ due to the non-monotonic nature of the $s_L(Z)$ curve. Finally, in this scenario, the value of $\bar{s}_L$ was forced to zero on both edges, which is the basic effect of using a value of $Z_{\min}$ or $Z_{\max}$ outside the flammable cloud to calculate the flame speed. See the Appendix for the FORTRAN source code used to calculate $\bar{s}_L$ and $\bar{s}_{L,M}$. This method had little effect on the magnitude of the transient peak in premixed combustion and reduced the premixed error to 2.3%. The cost increase of this version compared with the unmodified PPC formulation was just under 1%.

The time histories of the premixed and diffusion heat release rates are important in determining the success of the modification. In the unmodified case, the premixed heat release rate accounts for the majority of the total heat release rate over the entire domain (see Figure 3.3). When the $\bar{s}_L$ treatment is applied (Figure 3.7), the premixed heat release rate still accounts for a majority of the total heat release rate, but the magnitude of both have been significantly decreased. A look at the heat release rates in the upper portion of the domain, where we expect the premixed heat release rate to go to zero after the initial transient ignition phase, shows that the premixed heat release rate for the unmodified case has approximately the same magnitude as the diffusion heat release rate

in the quasi-steady state period (Figure 3.5). However, when the treatment is applied, the premixed heat release rate is reduced to near zero after the transient period (Figure 3.8). Similarly, a plot of the spatial distribution of the premixed and non-premixed heat release rate downstream of the premixed flame in the unmodified case (Figure 3.9) shows that the premixed heat release rate is not taken to zero, as we would expect. However, a similar plot for the modified case (Figure 3.10) shows that the premixed heat release rate has successfully been taken to zero at the same location downstream of the flame. This effect is well captured when viewing a pictorial representation of the premixed heat release rate field (Figure 3.11).

A comparison of the upper premixed heat release rate between the two treatments shows the overall effectiveness of the $\bar{s}_L$ algorithm (Figure 3.12). The treated premixed heat release rate has the desired result that the magnitude of the transient peak is approximately unchanged, while the quasi-steady state value goes to zero. The percent error, calculated as the fraction of the total heat release rate in the upper half of the domain, time-averaged over the quasi-steady state period, that is due to premixed combustion (see Eqn. (3-3)), gives an idea as to how effective the treatment was in reducing premixed combustion on the edges of the cloud. The percent error was approximately 2.3% in the treated case, versus nearly 50% in the untreated case.

Scatter plots of the flame speed and the reaction progress variable versus the mixture fraction show the effects of the model. In the unmodified case, the flame speed is not altered, and thus follows the quasi-parabolic approximation for the local flame speed

(Figure 3.13). When the treatment is applied however, $\bar{s}_L$ is forced to zero for some points, presumably those points determined to be edge conditions (Figure 3.14). The new quantity $\bar{s}_{L,M}$ introduced takes values along the prescribed curve for the local flame speed, except for areas outside the flammable cloud, or near its edge, where the values are higher than the prescribed relation (Figure 3.15). This demonstrates the desired effect that $\bar{s}_L$ is small and $\bar{s}_{L,M}$ is large near the edges of the flammable cloud. Furthermore, a comparison of the progress variable before (Figure 3.16) and after (Figure 3.17) the modification was applied shows that the higher values of $\bar{s}_{L,M}$ have successfully pushed the edge of the product cloud ($\tilde{c}$ = 1) to a region outside of the edge of the flammable cloud (as defined by the mixture fraction).

These trends are also evident in the spatial distribution of the flame speed and reaction progress variable, shown as a one-dimensional spatial variation through the center of the plume in Figures 3.18 and 3.19 and as pictorial representations in Figures 3.20 and 3.22. In these figures, we can see that the flame speed $\bar{s}_L$ is brought to zero near the edges of the flammable cloud, while the flame speed $\bar{s}_{L,M}$ takes high values at the edges. Note that both flame speeds take the same values in the central region away from the edges. Additionally, the decay of the progress variable has been successfully pushed to the outskirts of the cloud where the mixture fraction is below the lower flammable limit. The mixture fraction distribution is narrower and thus the region $\tilde{c}$ = 1 now encompasses the flammable range of the mixture fraction. Note that for the lower regions of the cloud, numerical error has caused the mixture fraction to be above the upper flammable limit.

This is the explanation for the odd behavior of $\bar{s}_L$ in Figure 3.20, as these regions qualified as edge conditions in the modified program, and the flame speed was therefore forced to zero.

In summary, the modified flame speed algorithm represents an improvement to the model. This modification allows the model to produce a qualitatively correct flame structure even for poorly-resolved simulations, thus allowing for larger-scale problems to be simulated in a reasonable time frame. This model also has the nice feature that for well-resolved cases ($\Delta \to 0$), the local variations in the mixture fraction are small and therefore $\bar{s}_L \to \bar{s}_{L,M}$. Therefore, the model reverts back to its original state for well-resolved cases while the new flame speed algorithm corrects errors in the premixed combustion for poorly-resolved cases, making the PPC model suitable for both research- and engineering-level use.

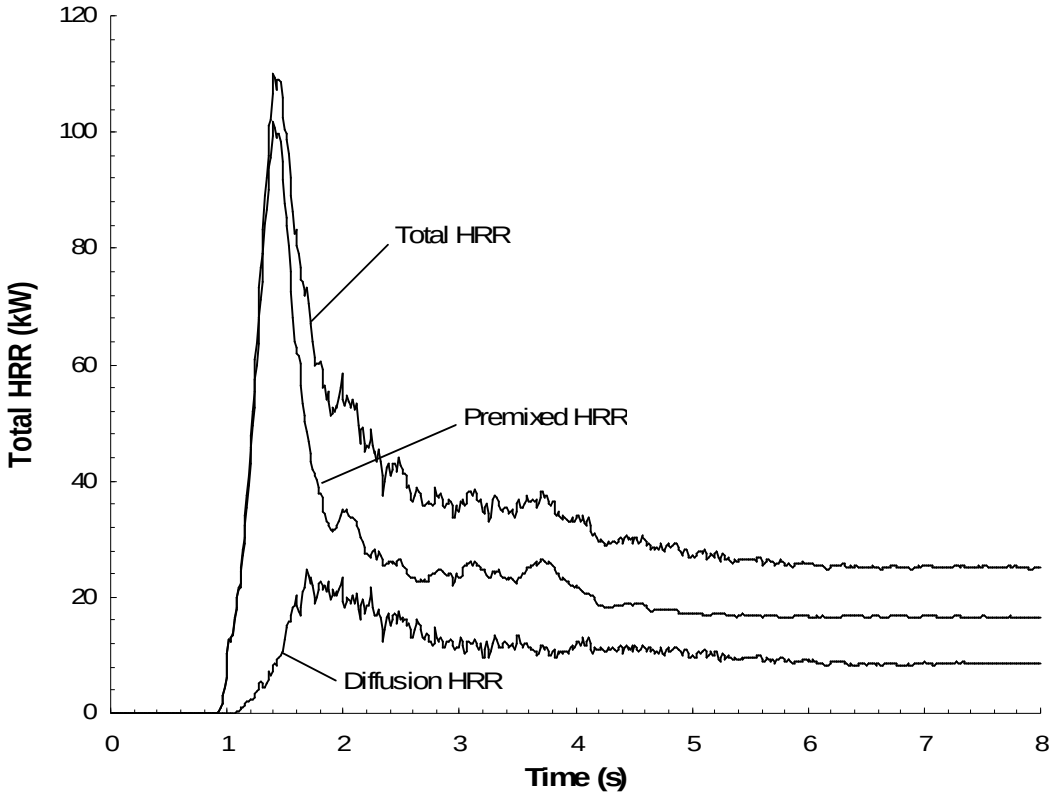

Figure 3.7: Total heat release rates for the $\bar{s}_L$-modified case.

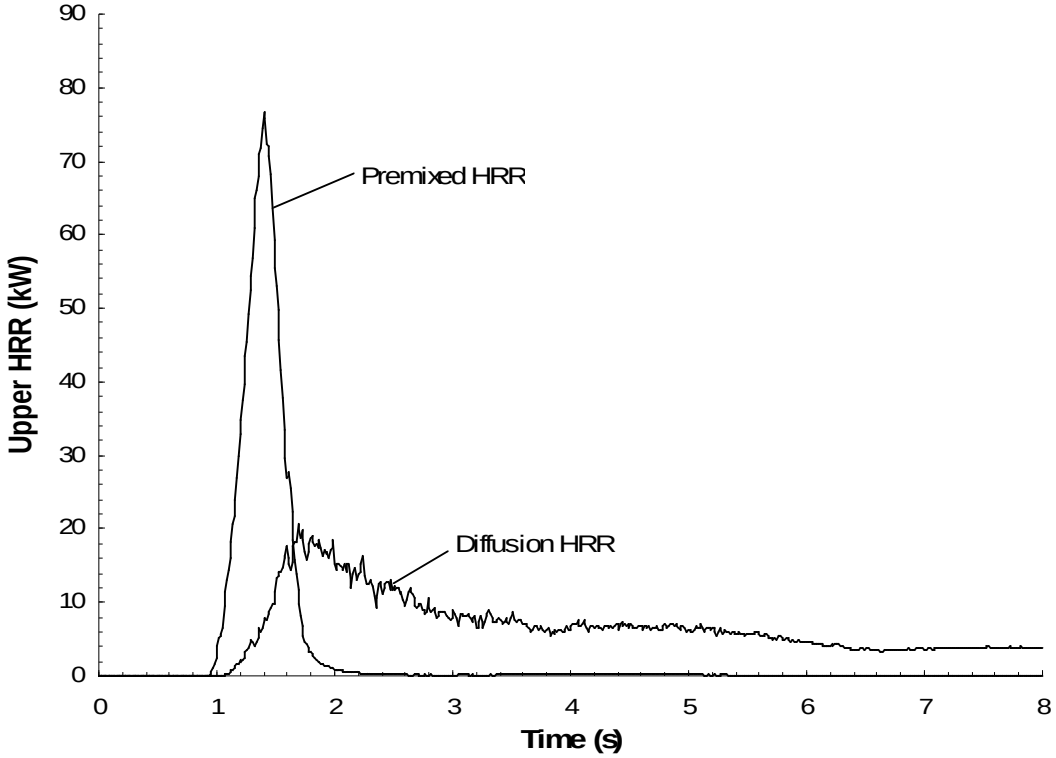

Figure 3.8: Heat release rate for the $\bar{s}_L$-modified case in the upper half of the domain

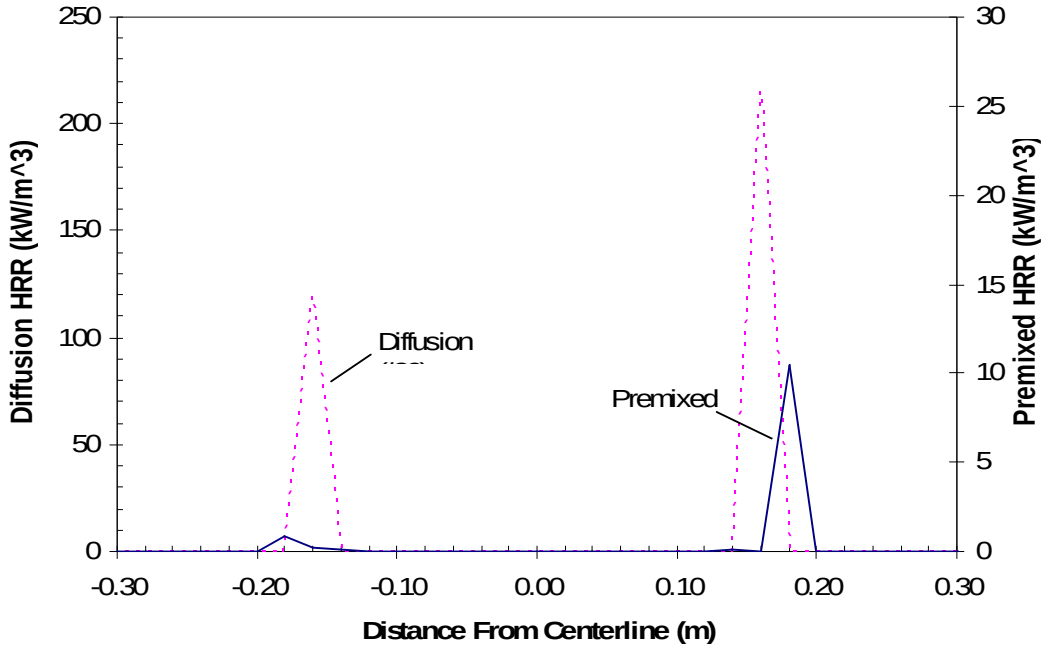

Figure 3.9: Profile of HRR components downstream of the premixed flame for the unmodified case. Profiles correspond to variations along the y = 0.72 m (center), z = 0.7 m line.

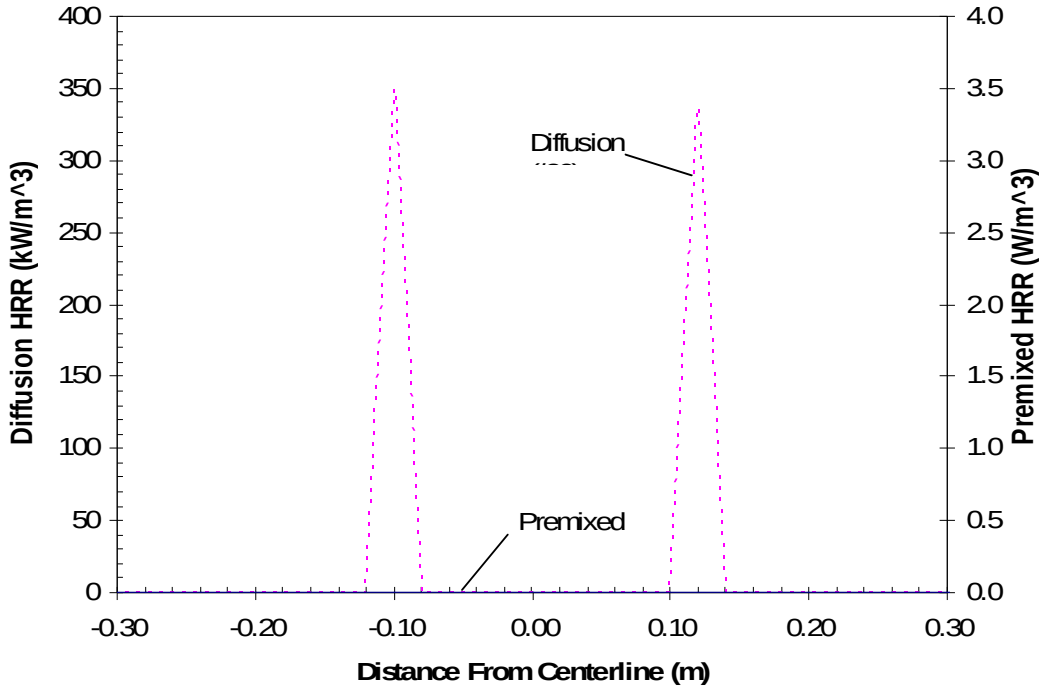

Figure 3.10: Profile of HRR components downstream of the premixed flame for the modified case. Profiles correspond to variations along the y = 0.72 m (center), z = 0.7 m line.

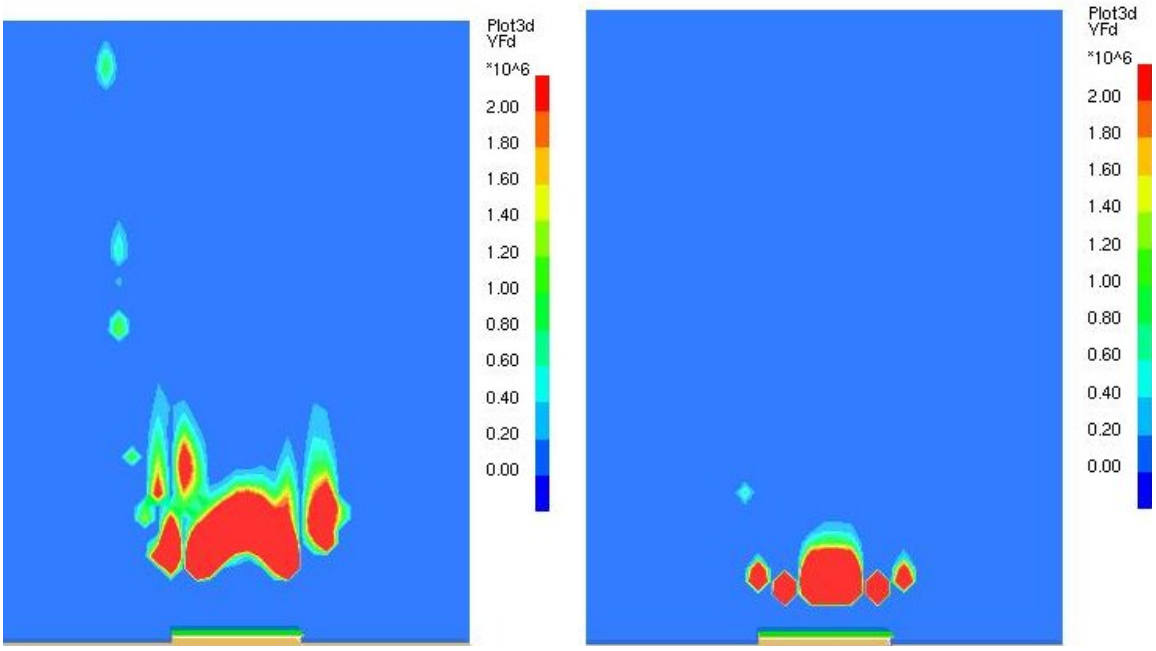

Figure 3.11: Distribution of the premixed heat release rate (W/m^3) without (left) and with (right) the $\overline{S}_L$ modification.

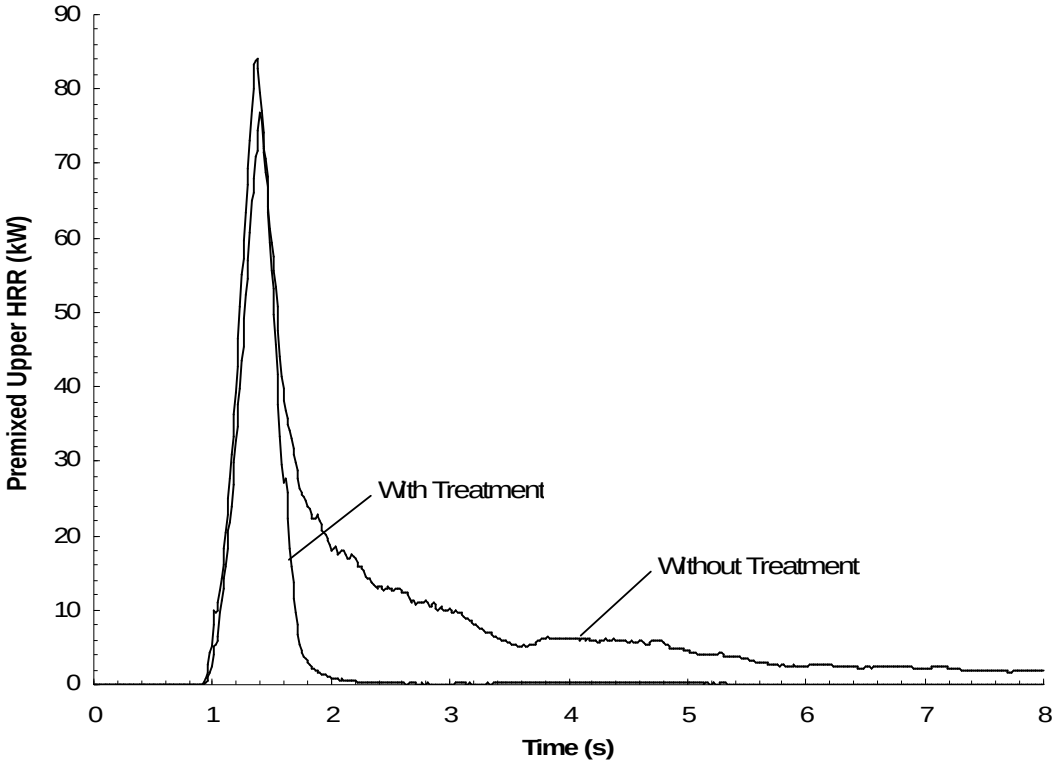

Figure 3.12: Effects of $\overline{S}_L$ treatment on premixed heat release rate in upper half of domain.

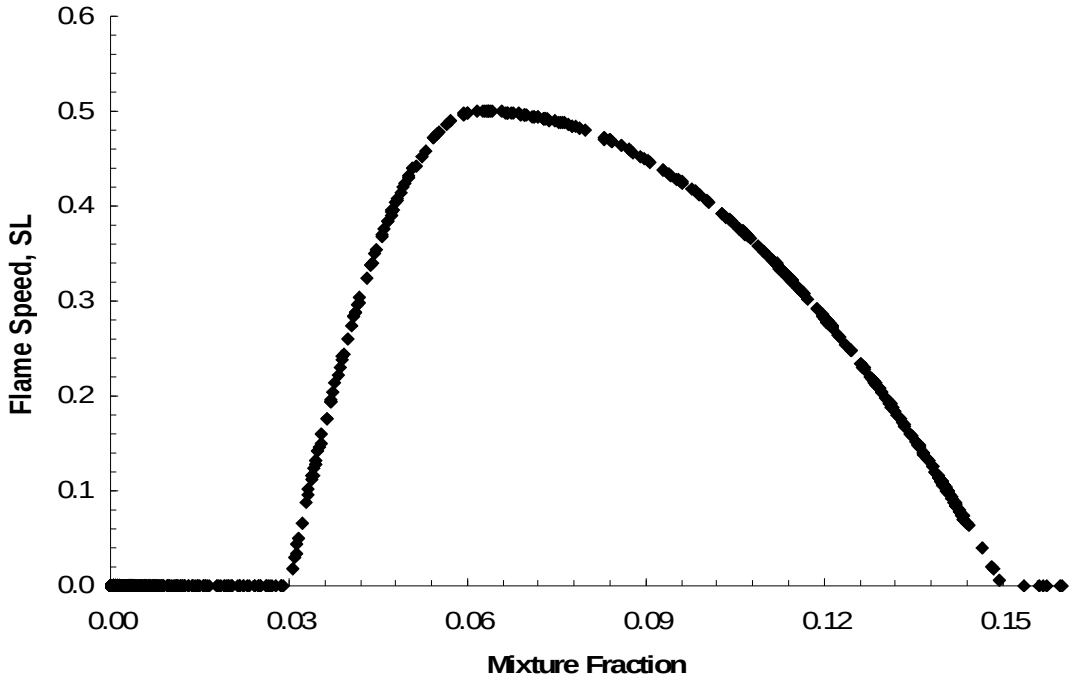

Figure 3.13: Flame speed s_L for the unmodified case. Profile corresponds to data in the plane z = 0.7 m.

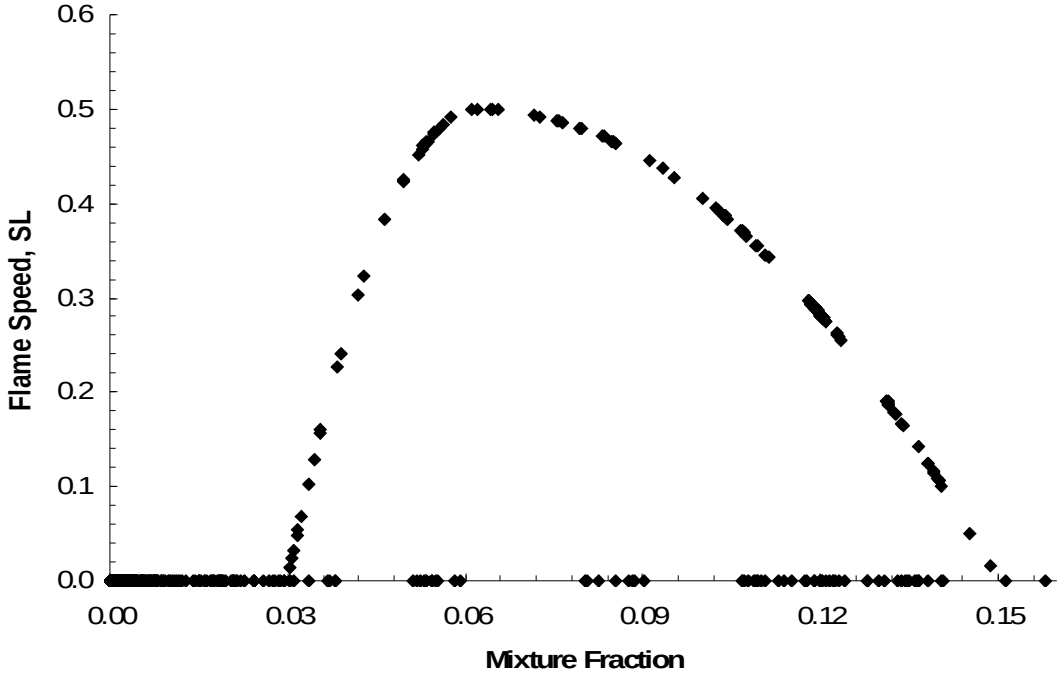

Figure 3.14: Flame speed $\bar{s}_L$ for the modified case. Profile corresponds to data in the plane z = 0.7 m.

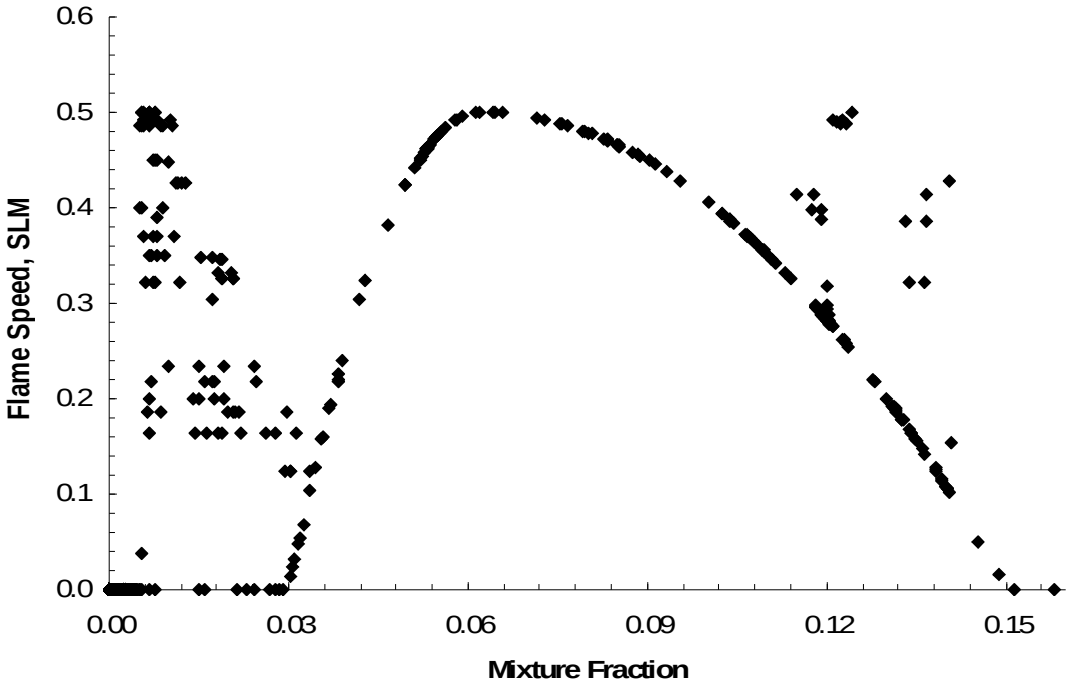

Figure 3.15: Flame speed $\bar{s}_{L,M}$ for the modified case. Profile corresponds to data in the plane z = 0.7 m.

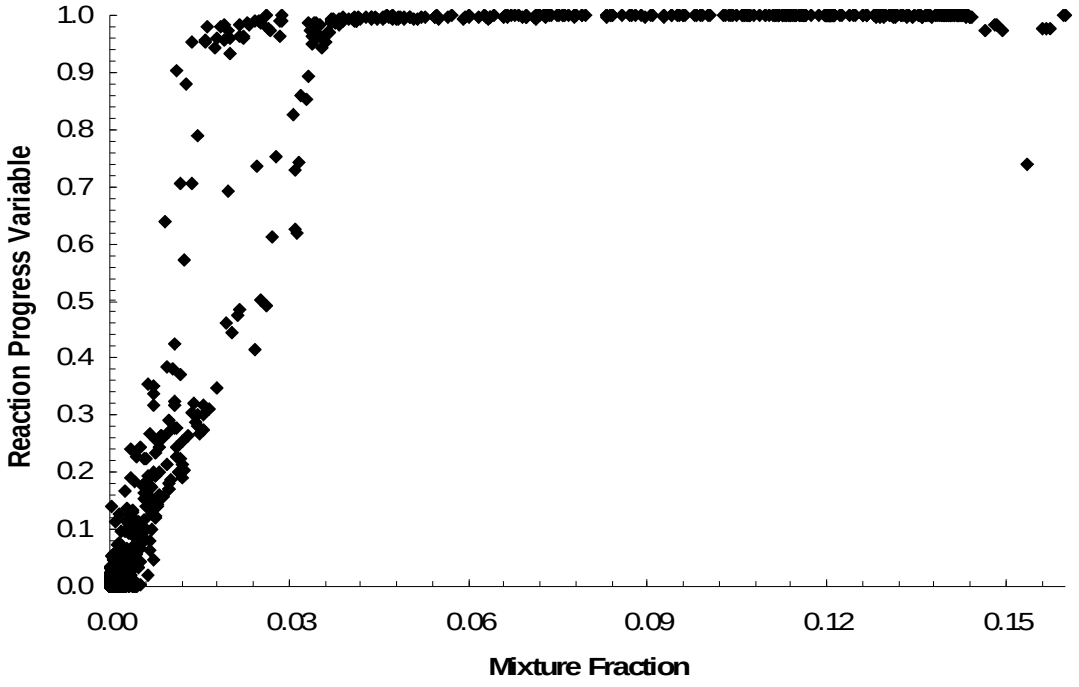

Figure 3.16: Reaction progress variable distribution over the mixture fraction for the upper region of the unmodified case. Profile corresponds to data in the plane z = 0.7 m.

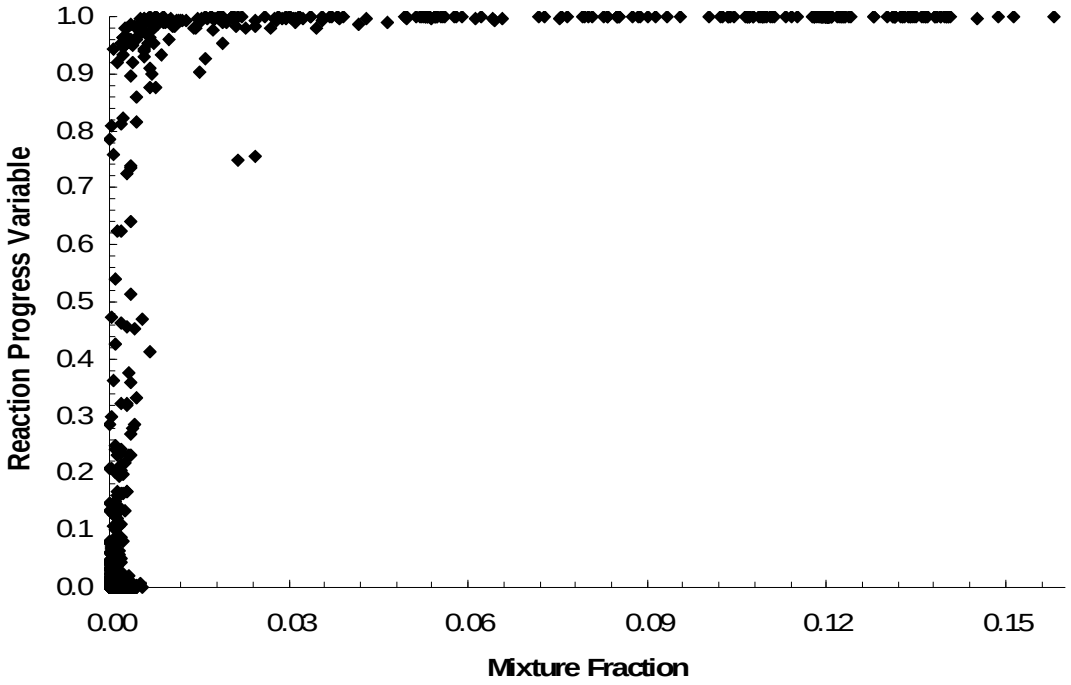

Figure 3.17: Reaction progress variable distribution over the mixture fraction for the upper region of the modified case. Profile corresponds to data in the plane z = 0.7 m.

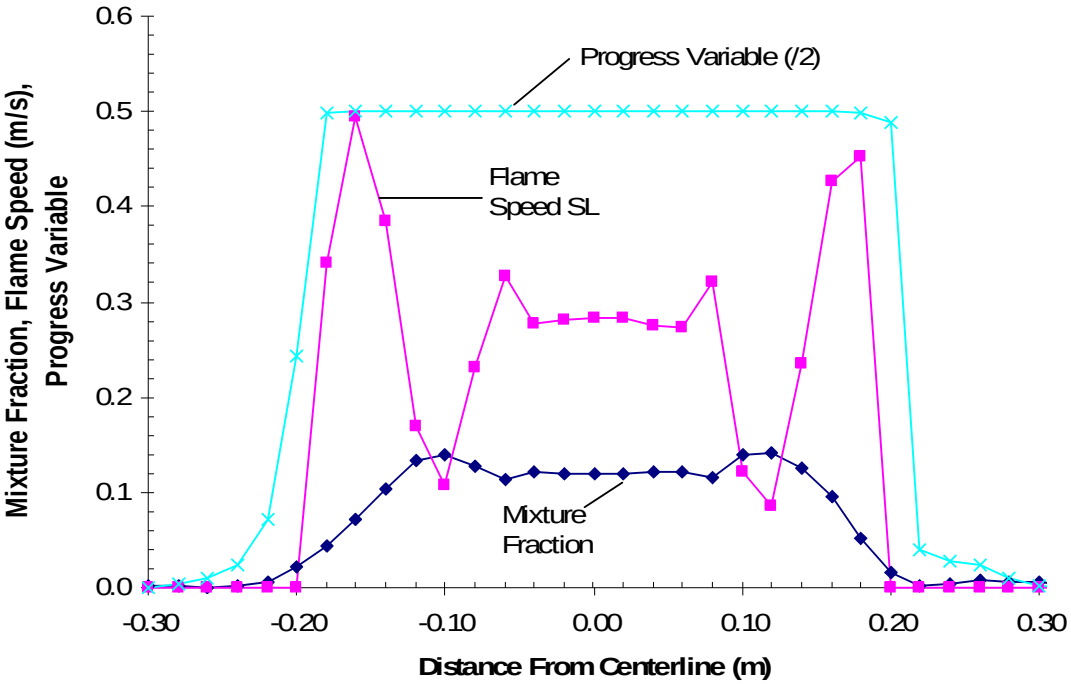

Figure 3.18: Profile of quantities of interest downstream of the premixed flame for the unmodified case. Profiles correspond to variations along the y = 0.72 m (center), z = 0.7 m line.

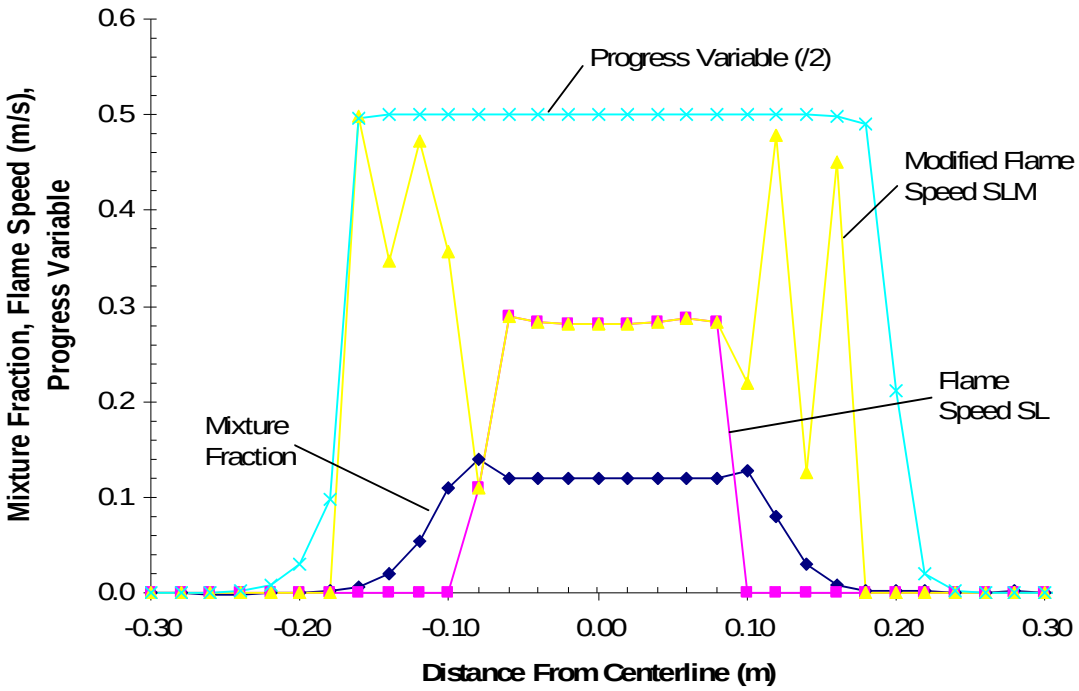

Figure 3.19: Profile of quantities of interest downstream of the premixed flame for the modified case. Profiles correspond to variations along the y = 0.72 m (center), z = 0.7 m line.

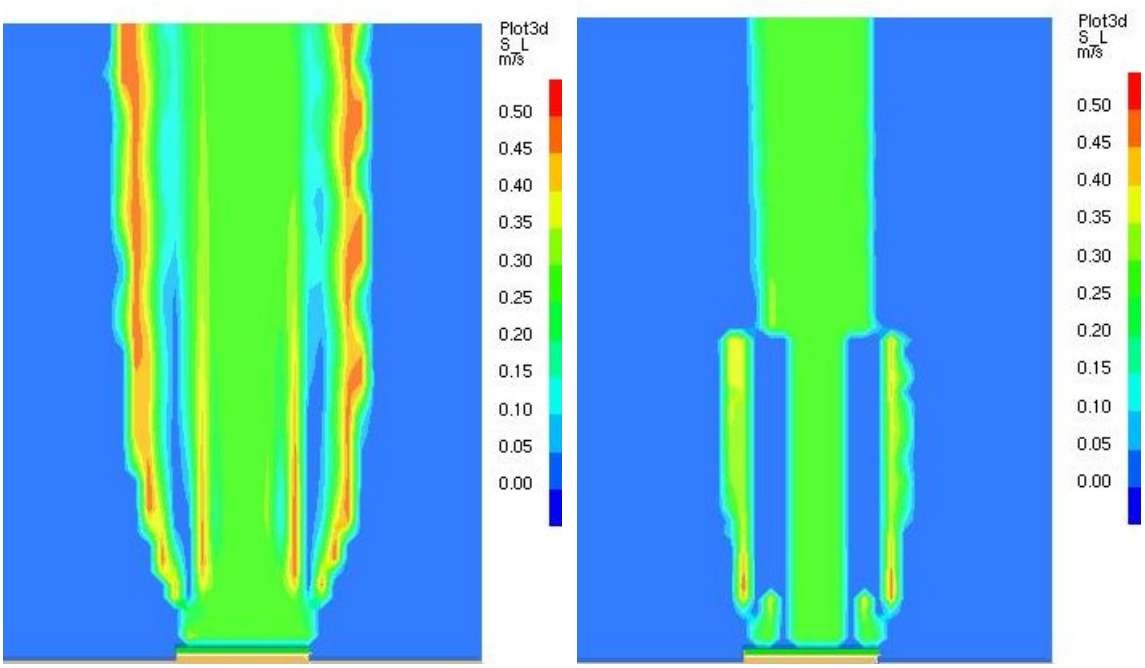

Figure 3.20: Distribution of the flame speed s_L (m/s) without (left) and with (right) the $\bar{s}_L$ modification.

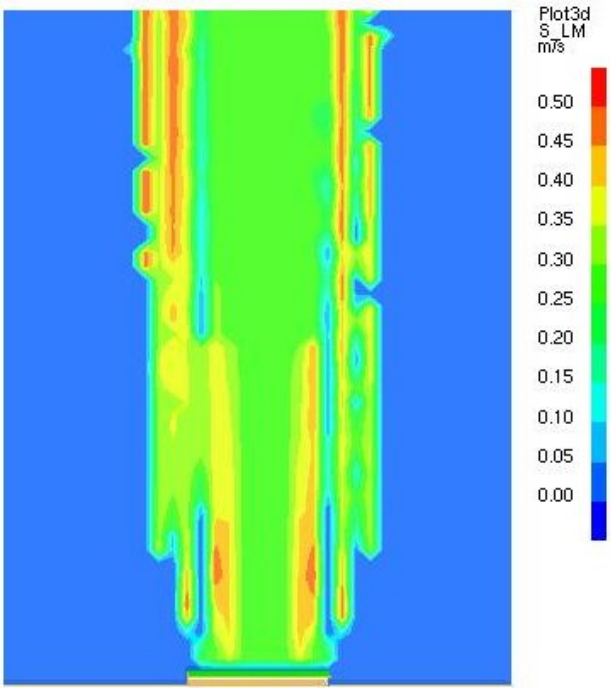

Figure 3.21: Distribution of the flame speed $\overline{S}_{L,M}$ (m/s) for the $\overline{S}_L$ -modified case.

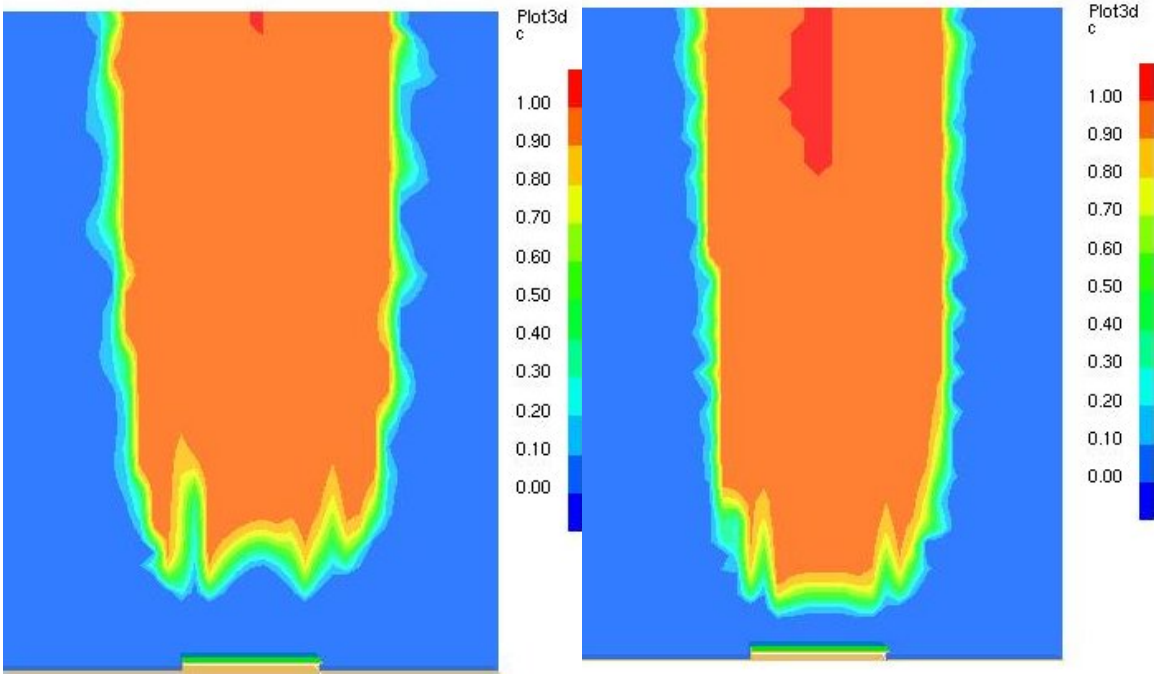

Figure 3.22: Distribution of the reaction progress variable without (left) and with (right) the $\overline{S}_L$ modification.

Chapter 4 Simulation of a Laminar Deflagration/Diffusion Flame Sequence

In order to stay abreast with recent developments to the Fire Dynamics Simulator, the PPC model has been implemented into Version 5 of FDS. In order to verify the model in this new context, the model was used to simulate a laminar deflagration-to-diffusion flame sequence. This simple configuration was used in order to first verify the success of the new model and was designed to be similar to verification experiments of the PPC model in the context of FDS4 [16]. The test configuration consists of a two-dimensional tunnel-like enclosure of dimensions 250 cm × 2.5 cm on a 500 × 5 grid for a computational grid size of $\Delta = 0.5$ cm. The boundary at $x = 0.0$ cm is specified as a solid boundary, while the boundary at $x = 250$ cm is fully open. Symmetry conditions are imposed for $z = 0.0$ cm and $z = 2.5$ cm. At initial time, the total mixture fraction is specified to correspond to monotonic variations from fuel-rich flammable conditions at large x-values, $Z_R = 0.12$, to pure air conditions at small x-values, $Z_L = 0$:

$$\widetilde{Z} = 0.5 \times \left[(Z_R + Z_L) + (Z_R - Z_L) \tanh(2(x - 0.5)/L_Z) \right] \tag{4-1}$$

where L_z is the gradient thickness of the $\widetilde{Z}$ -distribution.

The flame is ignited at time $t = 0.05$ s at the location $x = 250$ cm and propagates in the negative x-direction (into the solid boundary). This configuration ensures that the mixture fraction field is not significantly disturbed by thermal expansion due to

combustion. Propane is burned, with the following parameters for premixed combustion: $Z_{LFL} = 0.03,\ Z_{st} = 0.06,\ Z_{UFL} = 0.15,\ s_{L,st} = 0.5$ m/s. Results of the PPC model for a similar configuration tested in the context of FDS4 are presented in Ref. [16]. The model includes the changes made to the $\bar{s}_L$ algorithm presented in Chapter 3. Additionally, it is found that implementation of a binary flame index:

$$FI = \begin{cases} 0, & \nabla \widetilde{Y}_F . \nabla \widetilde{Y}_{O_2} \le 0 \\ 1, & \nabla \widetilde{Y}_F . \nabla \widetilde{Y}_{O_2} > 0 \end{cases} \tag{4-2}$$

rather than the continuous version described in Eqn. (2-23) provides a cleaner representation of the flame index and reduces errors caused by the new eddy dissipation model of non-premixed combustion, discussed below.

The time-dependent heat release rates are presented in Figure 4.1. After a short initial transient phase corresponding to ignition, the premixed flame undergoes a quasi-steady state as it travels through the region where $\widetilde{Z} \sim Z_R$. The premixed flame intensity then goes through a peak value as it passes through the stoichiometric mixture fraction surface and then decays to zero upon reaching the edge of the flammable cloud. As the premixed flame passes through the flammable fuel-rich region, unburned fuel is left behind due to lack of sufficient oxygen. Conversely, as the premixed flame passes through the flammable fuel-lean region, excess oxygen remains. When this residual fuel and oxygen mix, a diffusion flame develops at the stoichiometric mixture fraction surface after passage of the premixed flame. Thus this configuration corresponds to a two-stage

combustion process, starting with premixed burning and finishing with secondary diffusion burning.

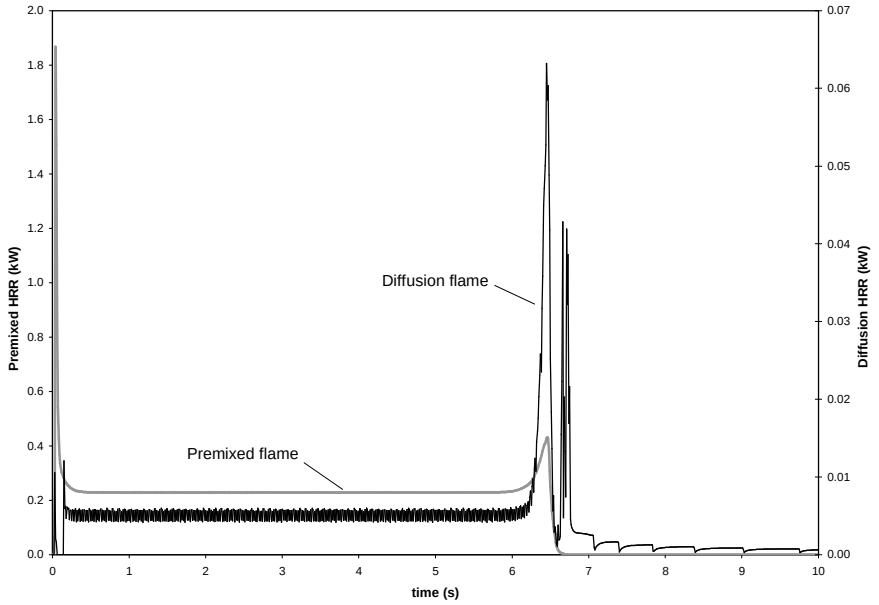

Figure 4.1: Time variations of the global premixed and diffusion heat release rates ($L_z / \Delta_c = 5$)

The diffusion heat release rate curve exhibits two unexpected features. The first is the existence of a diffusion flame during the initial quasi-steady state period, when combustion is expected to be entirely premixed. The second is the existence of a large peak in the diffusion burning rate (with respect to the quasi-steady state values) as the premixed flame passes through the non-zero mixture fraction gradient. A better understanding of these issues may be gained by studying the structure of the flame at time t = 6.24 s, just before the flame has reached the end of the $\widetilde{Z} \sim Z_R$ region (Figure 4.2). A trailing diffusion flame has developed in the wake of the premixed flame. The intensity of this diffusion burning is very high, on the same order of magnitude as the

premixed heat release rate, despite very low values of the oxygen concentration. The oxygen concentration corresponding to the peak intensity of diffusion burning is $Y_{O_2} = 0.0077$. Ideally, the oxygen concentration behind a premixed flame propagating though a fuel rich mixture would be zero. This non-zero mass of oxygen is the result of the reaction progress variable $\tilde{c}$ not reaching a value of exactly 1.

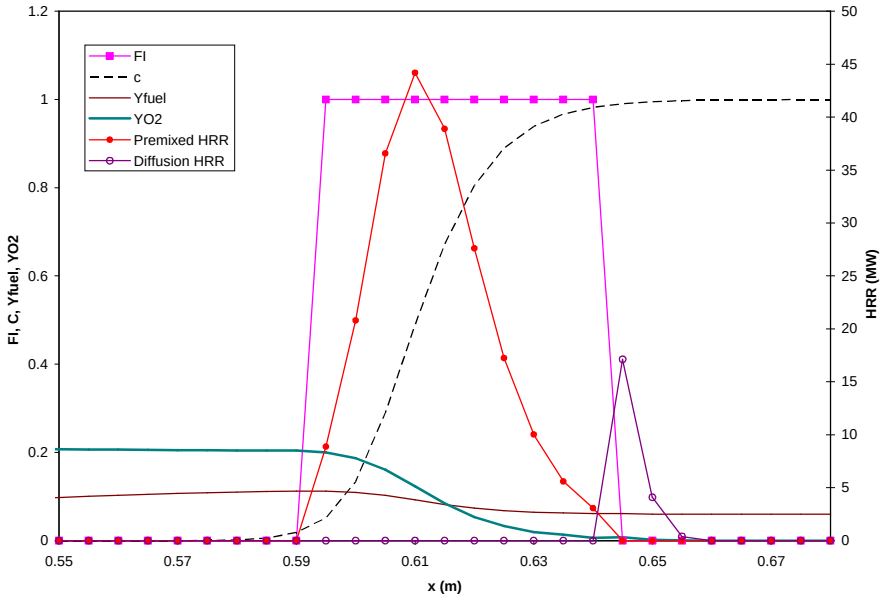

Figure 4.2: Details of the flame structure at t = 6.24 s. Fuel and oxygen concentrations shown are pre-combustion values ($L_z / \Delta_c = 5$).

The reason for this high-intensity diffusion flame has to do with the instantaneous nature of the diffusion model. The eddy dissipation combustion (EDC) model for non-premixed combustion implemented into FDS5 (Eqn. (2-18)) assumes that all fuel or oxygen in a computational grid cell is consumed in a single time step. For small time steps such as required for the PPC model (here $\delta t = 0.001$), this means that the diffusion burning rate

$\bar{\dot{q}}_d'''$ will be very high. Therefore, because the time step is a function of the computational grid cell size through the Courant-Friedrichs-Lewy (CFL) parameter, the instantaneous diffusion heat release rate may be a function of the grid cell size. Under quasi-steady state conditions for simple configurations, such as a jet diffusion flame, the EDC model should yield the correct burning rate regardless of grid cell size due to mass conservation restrictions. However, for transient events such as the one presently under consideration, the instantaneous diffusion burning rate will be grid-dependent.

This phenomenon also explains the violent diffusion burning just after the premixed flame has peaked. As the premixed flame passes through the region where $\widetilde{Z}$ varies from fuel-rich to fuel-lean, the diffusion flame has access to even greater amounts of fuel and oxygen, thus creating a large peak in diffusion burning as this fuel and oxygen is initially consumed. After this occurs, the expected quasi-steady state, mixing-controlled phase is established.

In order to eliminate the trailing diffusion flame as the premixed flame propagates through the region $\widetilde{Z} \sim Z_R$, the diffusion flame model has been modified to allow diffusion burning only when in the vicinity of the stoichiometric isosurface. In this way, the diffusion flame model of FDS5 is now more like the model of FDS4. To accomplish this, a search of the grid cells surrounding the cell of interest is performed to determine the minimum ($Z_{\min}$) and maximum ($Z_{\max}$) mixture fraction within a radius of 1 grid cell. Diffusion burning is then only allowed when the condition:

$$Z_{\min} \le Z_{st} \le Z_{\max} \tag{4-3}$$

is satisfied. The result of this change is presented in Figure 4.3. Compared to the previous formulation in Figure 4.1, this new formulation eliminates the diffusion flame during the quasi-steady period of the premixed flame (i.e. the trailing diffusion flame), and decreases the intensity of the peak diffusion burning rate.

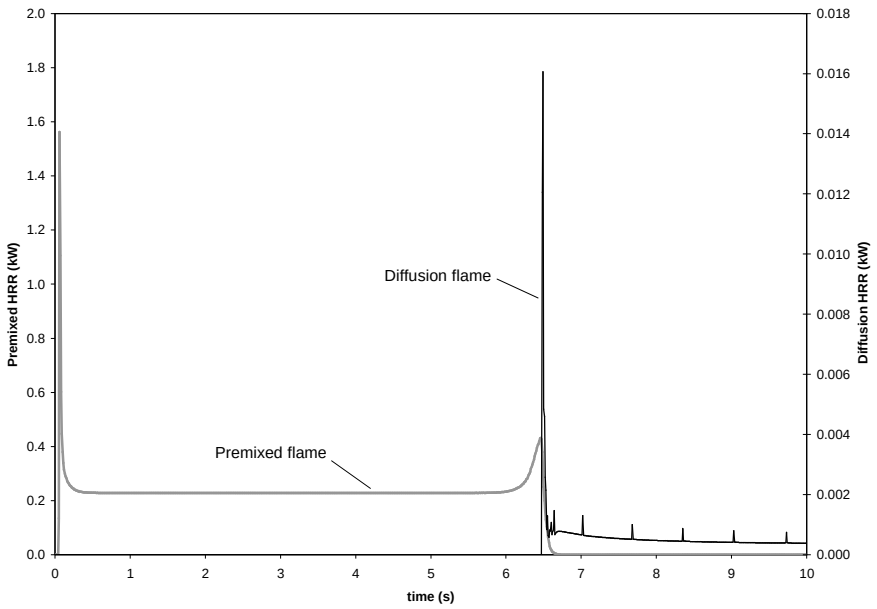

Figure 4.3: Time variations of the global premixed and diffusion heat release rates after the near-stoichiometry restriction is applied ($L_z / \Delta_c = 5$)

We next examine the effect of the stiffness of the $\widetilde{Z}$ -distribution on the results of the model. By varying the value of the ratio L_z / Δ_c, the premixed flame is either thick or thin compared to the gradient thickness of the $\widetilde{Z}$ -distribution. Because $\Delta_c = 5\Delta$ is held constant, this parameter can be viewed as a measure of the grid resolution, as the number

of grid cells over which the $\widetilde{Z}$-distribution is resolved will vary. Here we compare simulations performed with $L_z / \Delta_c = 5$ ($L_z = 25\Delta$) and $L_z / \Delta_c = 1$ ($L_z = 5\Delta$). In these simulations we keep the near-stoichiometry restriction previously discussed. The results of the calculation for $L_z / \Delta_c = 1$ are presented in Figure 4.4. When compared with the corresponding smooth $\widetilde{Z}$-distribution in Figure 4.3, the simulation with a stiff $\widetilde{Z}$-distribution is still capable of sustaining a diffusion flame in the quasi-steady mixing period, albeit at a higher intensity. In comparison with results previously generated in FDS4 [16], this represents an improvement, as previously $\widetilde{Z}$-distributions of this stiffness were not capable of sustaining a diffusion flame. The time-dependent premixed heat release rates are compared in Figure 4.5. When the $\widetilde{Z}$-distribution is smooth, the model is able to respond to the gradual variations in the mixture composition, and the premixed flame intensity reaches the theoretical maximum. When the $\widetilde{Z}$-distribution is stiff, the mixture composition varies too abruptly, and the peak value of the premixed burning is less than the theoretical maximum. It should be noted, however, that while some of the premixed burning is lost in this coarser distribution, the peak here is higher than that observed in the context of previous tests using FDS4 [16], representing an improvement in the model formulation.

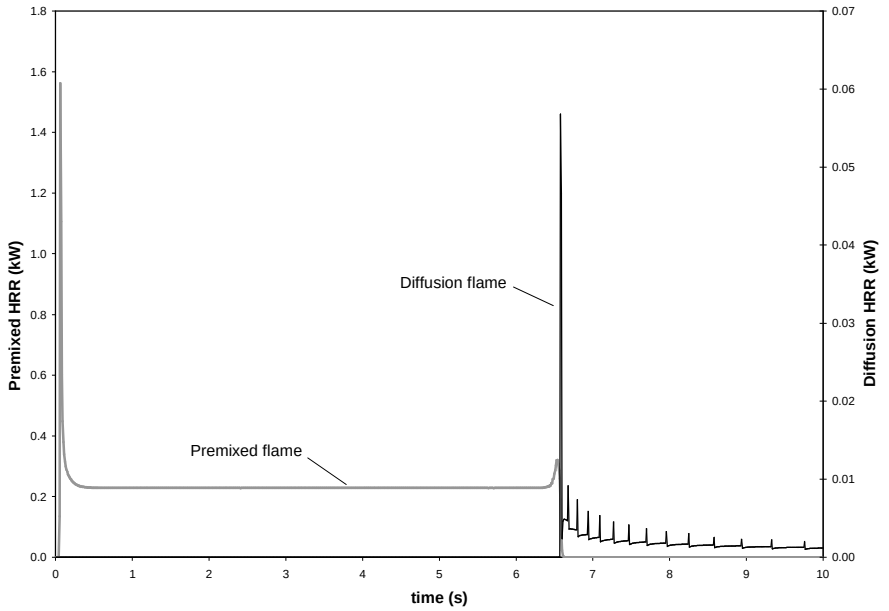

Figure 4.4: Time variations of the global premixed and diffusion heat release rates corresponding to a stiff $\widetilde{Z}$ -distribution, $L_z / \Delta_c = 1$

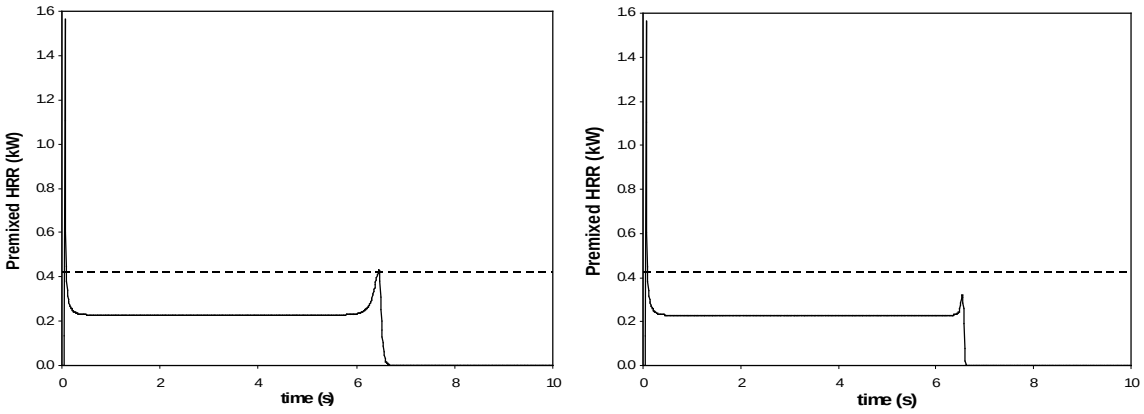

Figure 4.5: Time variations of the global premixed heat release rate. Left: smooth $\widetilde{Z}$ -distribution, $L_z / \Delta_c = 5$; right: stiff $\widetilde{Z}$ -distribution, $L_z / \Delta_c = 1$. The dashed line in both plots corresponds to the theoretical maximum premixed heat release rate for $\widetilde{Z} = Z_{st}$ and $s_L = s_{L,st}$

Chapter 5 Simulation of a Turbulent Deflagration/Diffusion Flame Sequence

We now seek to verify the changes to the model under a more complex testing configuration. The test configuration consists of a sealed compartment of size 4 m × 4 m × 3 m with an initial layer of heptane fuel near the floor (Figure 5.1). This floor layer corresponds to variations from a fuel-rich flammable mixture near the floor, $Z_R = 0.12$, to pure air conditions, $Z_L = 0$, around z = 0.5 m:

$$\widetilde{Z} = 0.5 \times \left[(Z_R + Z_L) - (Z_R - Z_L) \tanh((z - 0.5)/0.1) \right] \tag{5-1}$$

The total fuel mass is therefore 1.26 kg, with a stored combustion energy of 56 MJ (ΔH_F = 44.745 MJ/kg). This mixture is ignited at an off-center location (x,y,z) = (1.0,0.0,0.5) m at time t = 2 s. A square fuel leak of size 0.5 m × 0.5 m located at floor level in the center of the room leaks heptane fuel vapors into the room at a very small initial rate, which is then increased to that corresponding to a heat release rate of 500 kW once the flame has propagated back to the burner. The burner mass flow rate is kept initially small so that quasi-quiescent conditions are maintained before ignition. Consequently, this simulation represents a scenario in which a heavier-than-air fuel has leaked into a compartment and begun to accumulate near the floor before an ignition source is introduced. Upon ignition a premixed flame forms and propagates back

towards the fuel source, where it stabilizes as a diffusion flame. These simulations are similar to simulations presented in [16, 36].

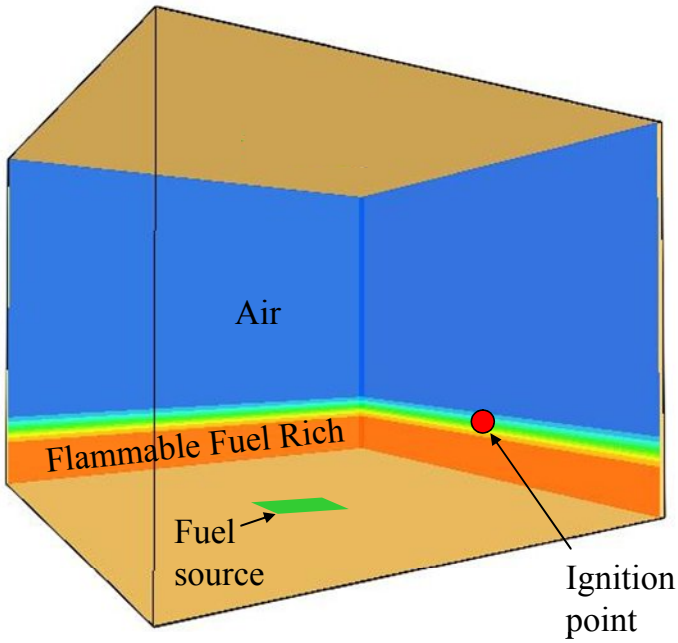

Figure 5.1: Sealed compartment test configuration. Shading along the back walls corresponds to the specified initial mixture fraction distribution.

The input parameters to the premixed combustion model are: $Z_{LFL} = 0.03$, $Z_{st} = 0.062$, $Z_{UFL} = 0.15$, $s_{L,st} = 0.5$ m/s. A uniform grid size of $\Delta = 0.025$ m on a side was used for a total grid of $160 \times 160 \times 120$ cells, and the computational domain is decomposed into 5 non-overlapping blocks. The walls are made of concrete. A light-back criterion is applied at the burner surface in order to allow transition to diffusion burning. A critical value of the reaction progress variable $\widetilde{c}_s$ is used to determine the time τ when the premixed flame has propagated back to the burner surface (here $\widetilde{c}_s$=0.6). Before light-back ($t \le \tau$), the mass loss rate (MLR) from the burner is small, $\dot{m}_F \approx 0.01\, g/s$, and the

incoming fuel mass is marked for premixed burning, $\widetilde{c} \approx 0$. In contrast, after light-back ($t > \tau$), the MLR is increased to $\dot{m}_F \approx 11.2\, g/s$, which corresponds to a heat release rate of 500 kW, and the incoming fuel mass is marked for a pure diffusion regime, $\widetilde{c} \approx 1$. This MLR is used to simulate a fuel source that continues to leak at the defined rate after the initial fuel cloud is consumed.

It was also necessary to make a slight change to the $\bar{s}_L$ algorithm presented in Chapter 3. The previous algorithm was not applied to points satisfying the condition $Z_{\min} \le Z_{UFL} \le Z_{LFL} \le Z_{\max}$ in order to prevent the elimination of the premixed flame in the case of coarse grids where the mixture fraction is not well-resolved over the 2 grid cell search region. It is found, however, that this method does not enforce a transition to strictly diffusion burning in the case of light-back, where the $\widetilde{Z}$-distribution is stiff. The following condition was therefore added to the $\bar{s}_L$ algorithm:

$$\begin{aligned} &If: Z_{\min} \le Z_{UFL} \le Z_{LFL} \le Z_{\max} \\ &Then: \bar{s}_L = \bar{s}_{L.M} = s_{L,st} \end{aligned} \tag{5-2}$$

This model has the desired effect of allowing premixed burning during the transient phase, while enforcing a transition to strictly diffusion burning after light-back. This change to the $\bar{s}_L$ algorithm is reflected in the source code presented in the Appendix.

To facilitate a discussion of the flame dynamics, a series of iso-surfaces generated using the FDS5 version of the non-premixed combustion model is presented in Figures 5.2 - 5.4

corresponding to the premixed and diffusion burning locations at two different times: t = 2.5 s and t = 3.5 s. A similar result is presented in the context of FDS4, and without any of the model improvements discussed here, in Ref. [36]. In the first set of images, (Figure 5.2), it is evident that the premixed flame propagates dominantly horizontally, while the diffusion flame is moved upward by buoyant forces and forms a fireball ("mushroom cloud"). At a later time (Figure 5.3), the premixed flame has continued to spread horizontally and has impinged upon the sidewall, while the diffusion flame is now impinging upon the ceiling of the enclosure. These events are sufficient to cause a transition to turbulence, and there follows a time period where the combustion topology becomes chaotic and shows no clear flame structure. This period ends with the establishment of a quasi-steady diffusion flame at the burner (Figure 5.4). These results are qualitatively consistent with previously observed results generated in FDS4 [36].

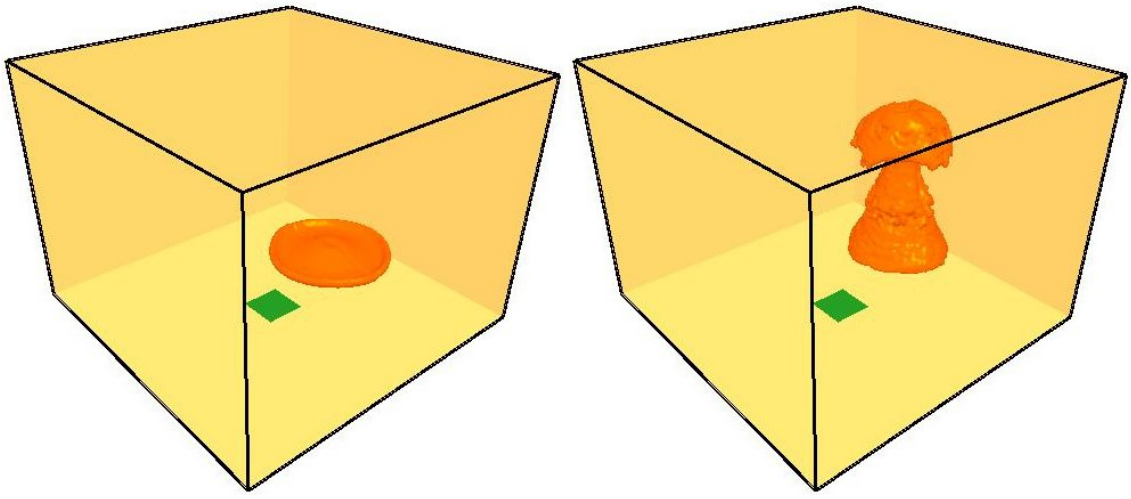

Figure 5.2: Instantaneous iso-surfaces showing the premixed (left; $(FI \times \dot{\bar{q}}_p''') = 5\ \mathrm{MW/m^3}$) and diffusion (right; $(1-FI)\, f_{ign} \times \dot{\bar{q}}_d''' = 100\ \mathrm{kW/m^3}$) components of the heat release rate at time t = 2.5 s.

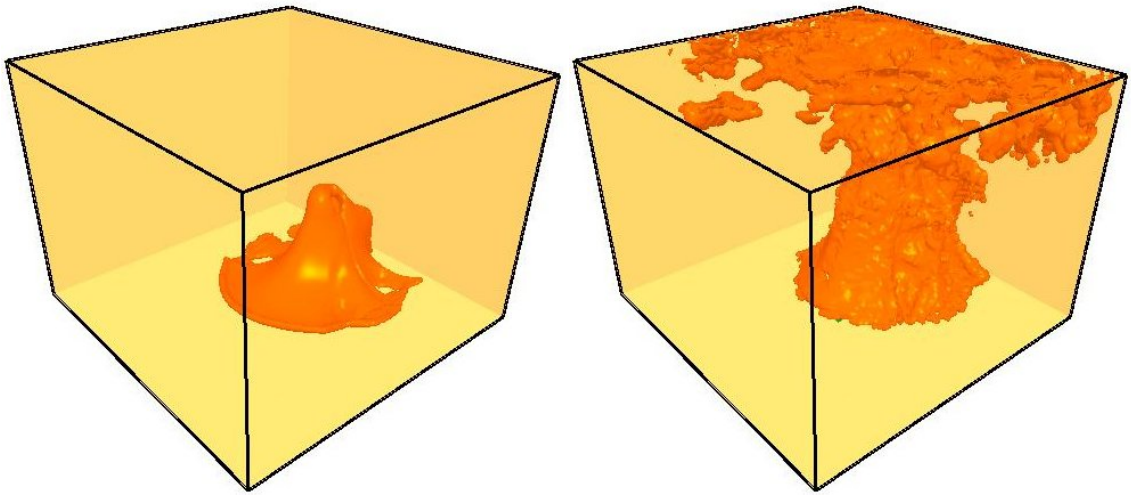

Figure 5.3: Instantaneous iso-surfaces showing the premixed (left; $(FI \times \bar{\dot{q}}_p''') = 5\ \mathrm{MW/m^3}$) and diffusion (right; $(1-FI)\, f_{ign} \times \bar{\dot{q}}_d''' = 100\ \mathrm{kW/m^3}$) components of the heat release rate at time t = 3.5 s.

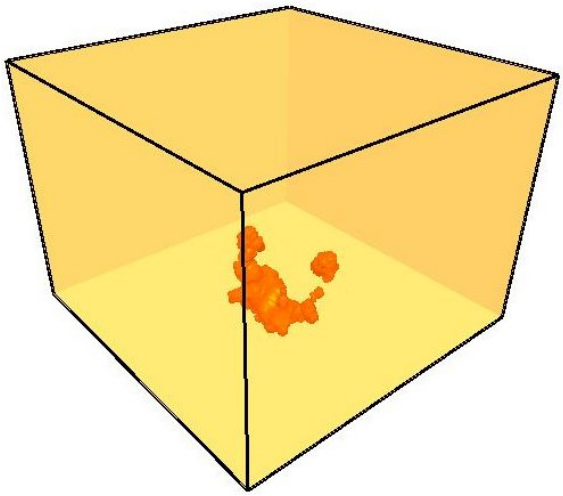

Figure 5.4: Instantaneous iso-surface showing the diffusion ($(1-FI)\, f_{ign} \times \bar{\dot{q}}_d''' = 100\ \mathrm{kW/m^3}$) component of the heat release rate at time t = 8.5 s.

The flame dynamics are reflected in the time-dependent heat release rate data in Figure 5.5. The premixed heat release rate increases immediately after ignition at t = 2 s, followed shortly afterward by the diffusion heat release rate. The transient partially-

premixed combustion phase lasts only a short time, after which the premixed heat release rate is zero or near-zero, and the diffusion heat release rate is approximately 500 kW, as specified by the fuel mass loss rate.

Figure 5.5 shows the effects of the new $\bar{s}_L$ and binary flame index algorithms on the global heat release rates in the context of FDS4. The effect of the modifications is to decrease the peak premixed burning rate. This is because the $\bar{s}_L$ model has eliminated the premixed burning at the edge of the product plume, as demonstrated in Figure 5.6. However, according to the algorithm, a portion of the initial fuel layer, near the lower flammable limit, is also considered an edge and therefore the premixed burning is suppressed here as well. As a result, the diffusion flame peak is slightly higher as some of the fuel originally burned by the premixed flame is now burned by the diffusion flame. Also note that, as a result of the new algorithm, the premixed flame intensity goes to zero after the initial transient period, rather than slowly decaying to zero over a period of several seconds as before.

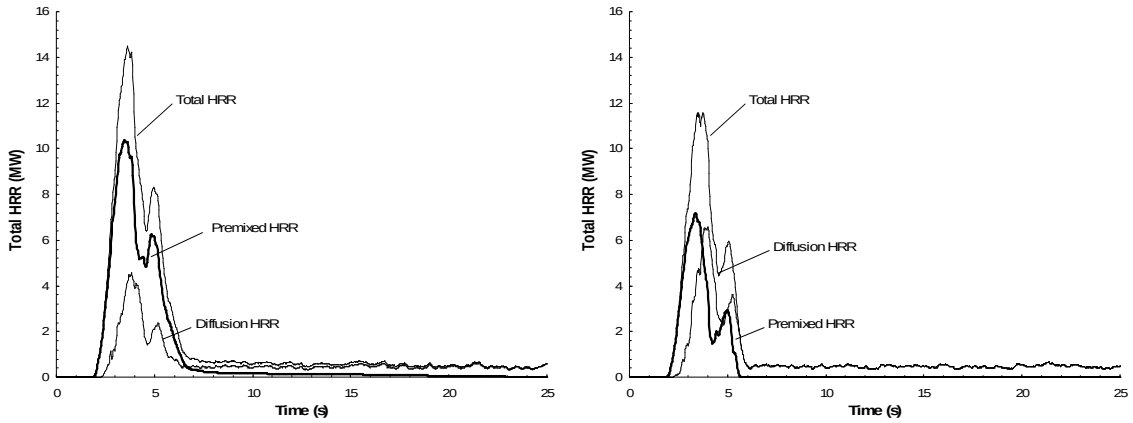

Figure 5.5: Time variations of the global heat release rates in the sealed compartment calculated using FDS4 without (left) and with (right) new $\bar{s}_L$ and flame index modifications.

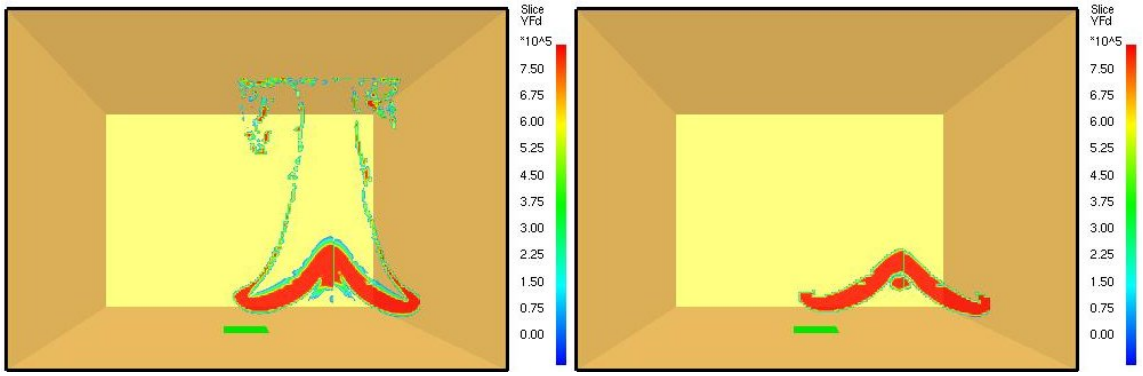

Figure 5.6: Instantaneous distribution of the premixed heat release rate (W/m^3) for the plane y = 0 at time t = 2.75 calculated using FDS4 without (left) and with (right) new $\bar{s}_L$ and flame index modifications.

When the FDS5 version of the solver is used, including the $\bar{s}_L$ algorithm, binary flame index, and the near-stoichiometry restriction, the results are significantly different. Figure 5.7 shows the time variations of the heat release rate obtained using this version of the solver. The premixed flame peak is of approximately the same intensity as the comparable simulation in FDS4 (Figure 5.5b). However, the diffusion flame peak is considerably higher than previously observed. The reason for this difference lies in the

combination of the new $\bar{s}_L$ algorithm and the new non-premixed combustion model in FDS5. As previously mentioned, the $\bar{s}_L$ algorithm determines a part of the initial fuel layer to be a lean edge condition. While this edge condition only penetrates a few grid cells into the depth of the layer, this represents a non-trivial amount of fuel, due to the stiff $\widetilde{Z}$-distribution. Therefore, since these points are determined to be edges, the algorithm sets the premixed heat release rate to zero while enhancing the propagation of the reaction progress variable through this region. Since the algorithm artificially enhances the propagation of the reaction progress variable, this allows f_{ign} (an ignition factor that limits diffusion burning to post-premixed combustion) to be non-zero and thus the remaining unburned fuel and oxygen is burned very rapidly in diffusion mode as described previously (Chapter 4) for the tunnel case. In combination, this leads to low values of the premixed heat release rate and high values of the diffusion heat release rate. This augmentation of the diffusive burning is supported by a comparison of instantaneous spatial variations of the diffusion heat release rate (Figure 5.8), where it is seen that the FDS5 version exhibits more intense diffusive burning than its FDS4 counterpart.

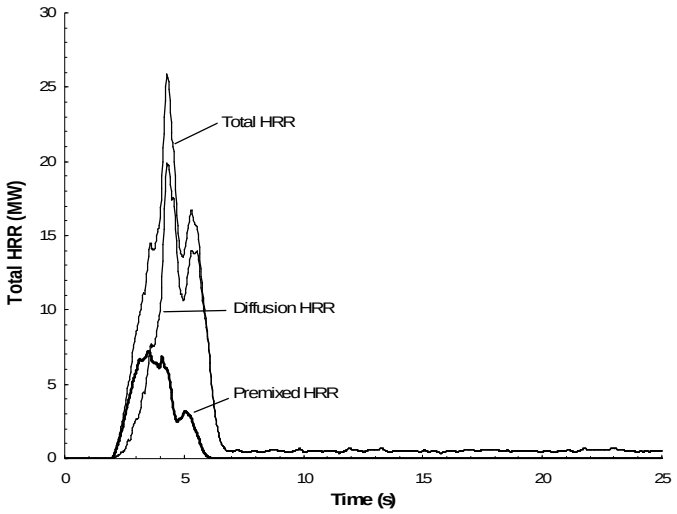

Figure 5.7: Time variations of the global heat release rates in the sealed compartment calculated using FDS5 with new $\bar{S}_L$, flame index, and near-stoichiometry modifications.

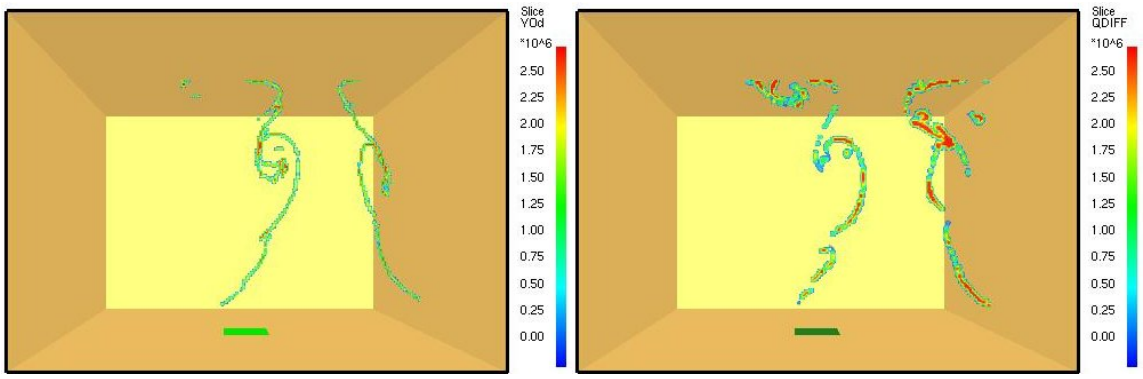

Figure 5.8: Instantaneous distribution of the diffusion heat release rate (W/m^3) for the plane y = 0 at time t = 3.0 calculated using FDS4 (left) and FDS5 (right), both with new $\bar{S}_L$ and flame index modifications

Chapter 6 Conclusion

A partially-premixed combustion (PPC) capability has been implemented into the Fire Dynamics Simulator (FDS) model. The model is based on a Large Eddy Simulation (LES) approach and uses a reaction progress variable concept to describe premixed combustion and either a mixture-fraction based model (FDS4) or an eddy dissipation model (FDS5) is used to describe non-premixed combustion. The results obtained using these two non-premixed combustion models are compared. An LES-resolved flame index is used to couple the premixed and the non-premixed combustion modes. This model is capable of simulating ignition and combustion in partially-premixed combustion scenarios.

The present study is focused on reducing the grid resolution requirement for the partially-premixed combustion model so that the model is capable of simulating partially-premixed combustion on the large scales of interest to the engineer at a reasonable computational cost. A new algorithm for the laminar flame speed is shown to be successful at limiting the errors in premixed combustion arising from diffusion of the reaction progress variable at the edge of the product cloud when coarse computational grids are used. The result of this modification is that the PPC model is less grid-dependent, making it suitable for both research- and engineering-level use. Additionally, the model is shown to capture the flame dynamics of a deflagration/diffusion flame sequence in the context of the new Version 5 of the Fire Dynamics Simulator, albeit with

a considerably higher diffusion flame intensity due to the new eddy-dissipation model used for non-premixed combustion.

These results are encouraging for the application of the model to modern engineering fire problems. Efforts are currently under way to validate the model against experiments conducted by Factory Mutual Research Corporation in 1999 that are similar in design to the sealed compartment simulations presented in Chapter 5. Future work will focus on further validation the model against experimental data. Another focus of further research will be to explore the application of the model to large-scale outdoor fuel vapor cloud fires, such as those resulting from liquefied natural gas (LNG) tanker leaks, and indoor backdraft phenomena.

Appendix: FORTRAN Code for Calculation of $\bar{s}_L$ and $\bar{s}_{L,M}$

```
      CALC_SL: IF (PREDICTOR) THEN

C     Note: here YYP(I,J,K,1) represents the local mixture fraction, ZL
C     is the lower flammable mixture fraction, and ZR is the upper
C     flammable mixture fraction

      IF (LES) THEN   ! Smagorinsky model (LES)
C
        S_L  = 0.
        S_LM = 0.
C
      KLOOPb: DO K=1,KBAR
      JLOOPb: DO J=1,JBAR
      ILOOPb: DO I=1,IBAR
        IF (SOLID(ICA(I,J,K))) CYCLE ILOOPb
        IF ( (YYP(I,J,K,1).lt.0.005).or.(YYP(I,J,K,1).gt.0.995) )
     &        CYCLE ILOOPb
C
C Calculate unmodified local flame speed
        If( (YYP(I,J,K,1).gt.ZL).and.(YYP(I,J,K,1).le.Zst) ) then
           S_L(I,J,K) = S_Lst*(1.-((Zst-YYP(I,J,K,1))/(Zst-ZL))**2.)
        Endif
        If( (YYP(I,J,K,1).gt.Zst).and.(YYP(I,J,K,1).lt.ZR) ) then
           S_L(I,J,K) = S_Lst*(1.-((YYP(I,J,K,1)-Zst)/(ZR-Zst))**2.)
        Endif
        S_LM(I,J,K)= S_L(I,J,K)
C
C Find ZMIN and ZMAX over the range plus/minus 2 grid cells in each
direction
        ZMIN      = 1.
        ZMAX      = 0.
        KLOOPc: DO KK=MAX(1,K-2),MIN(KBAR,K+2)
        JLOOPc: DO JJ=MAX(1,J-2),MIN(JBAR,J+2)
        ILOOPc: DO II=MAX(1,I-2),MIN(IBAR,I+2)
          IF (SOLID(ICA(II,JJ,KK))) CYCLE ILOOPc
          ZMIN = MIN(YYP(II,JJ,KK,1),ZMIN)
          ZMAX = MAX(YYP(II,JJ,KK,1),ZMAX)
        ENDDO ILOOPc
        ENDDO JLOOPc
        ENDDO KLOOPc
C
C Edges treatment
        xstore1 = (ZMIN-ZL)*(ZMAX-ZL)*(ZMIN-ZR)*(ZMAX-ZR)
C
        If (xstore1.lt.0.) Then
           xstore4 = (ZMIN-ZL)*(ZMAX-ZL)
           If (xstore4.lt.0.) Then
              xstore2 = ZMIN
              xstore3 = ZMAX
           Else
              xstore2 = ZMAX
              xstore3 = ZMIN
```

```
            Endif
C
            S_L(I,J,K) = 0.
            If( (xstore3.gt.ZL).and.(xstore3.le.Zst) ) then
               xstore4 = S_Lst*(1.-((Zst-xstore3)/(Zst-ZL))**2.)
            Endif
            If( (xstore3.gt.Zst).and.(xstore3.lt.ZR) ) then
               xstore4 = S_Lst*(1.-((xstore3-Zst)/(ZR-Zst))**2.)
            Endif
            S_LM(I,J,K) = MAX(S_LM(I,J,K),xstore4)
C
         Endif
C
         If (  (((ZMIN-ZL)*(ZMAX-ZL)).le.0.)
     &     .and.(((ZMIN-ZR)*(ZMAX-ZR)).le.0.)  ) Then
           S_L(I,J,K) = S_Lst
           S_LM(I,J,K) = S_Lst
         Endif
C
       ENDDO ILOOPb
       ENDDO JLOOPb
       ENDDO KLOOPb
C
       ENDIF
       ENDIF CALC_SL
```

Nomenclature

A	area of the burner (m^2)
$\widetilde{c}$	filtered reaction progress variable (-)
c^*	reaction progress variable for non-premixed combustion (-)
$\widetilde{c}_s$	critical reaction progress variable for light-back (-)
D	mass molecular diffusion coefficient (m^2/s)
δt	time step (s)
Δ	computational grid size (m)
Δ_c	LES filter size for *c*-equation (m)
ΔH_F	heat of combustion (kJ/kg)
FI	LES-resolved flame index (-)
L_z	characteristic mixture fraction gradient length scale (m)
ν_t	Smagorinsky turbulent eddy-diffusivity (m^2/s)
$\widetilde{p}(Z_{st})$	stoichiometric value of the (Favre-weighted) Pdf that describes subgrid-scale variations in *Z* (-)
$\overline{\dot{q}}'''$	total local volumetric heat release rate (W/m^3)
$\overline{\dot{q}}_d'''$	local volumetric non-premixed heat release rate (W/m^3)
$\overline{\dot{q}}_p'''$	local volumetric premixed heat release rate (W/m^3)
$\dot{Q}$	total global heat release rate (W)
r_s	stoichiometric oxygen-to-fuel mass ratio (kg/kg)
ρ	local density (kg/m^3)
ρ_u	density of unburned gases (kg/m^3)
Sc_t	turbulent Schmidt number (-)
s_L	local laminar flame speed (m/s)
$s_{L,st}$	stoichiometric vale of the laminar flame speed (m/s)
$\overline{s}_L$	modified laminar flame speed, featuring a reduced burning rate near the edges of the flammable cloud (m/s)
$\overline{s}_{L,M}$	modified laminar flame speed, featuring enhanced propagation near the edges of the flammable cloud (m/s)
Σ	LES-filtered flame surface density (m^{-1})
τ	light-back time (s)
u_0	fuel/air supply velocity (m/s)
u_i	is the x_i-component of the flow velocity vector (m/s)
$\dot{\omega}_c$	reaction rate of *c* per unit volume ($kg/s\text{-}m^3$)
$\overline{\dot{\omega}}_F$	mass reaction rate of fuel per unit volume ($kg/s\text{-}m^3$)
W_k	molecular weight of species *k* (g/mol)
x,y,z	three-dimensional Cartesian coordinates (m)
Ξ	subgrid-scale flame wrinkling factor (-)

$\widetilde{\chi}$ LES-filtered scalar dissipation rate

$Y_{f,0}$ mass fraction of fuel in the burner fuel jet (-)

Y_F^{∞} mass fraction of fuel in the fuel supply stream (-)

Y_k mass fraction of species *k* (-)

Y_k^m mass fraction of species *k* in the unburned gas (-)

Y_k^{eq} mass fraction of species *k* in the burned gas (-)

$\widetilde{Z}$ mixture fraction (-)

Z_{LFL} lower flammable mixture fraction (-)

$Z_{\max}$ local maximum mixture fraction (-)

$Z_{\min}$ local minimum mixture fraction (-)

Z_{st} stoichiometric value of the mixture fraction (-)

Z_{UFL} upper flammable mixture fraction (-)

Bibliography

[1] K. McGrattan, "Fire Dynamics Simulator (Version 4) Technical Reference Guide," National Institute of Standards and Technology, Gaithersburg, MD, NIST Special Publication 1018, 2004.

[2] K. McGrattan, H. Baum, R. Rehm, S. Hostikka, and J. Floyd, "Fire Dynamics Simulator (Version 5) Technical Reference Guide (Draft)," National Institute of Standards and Technology, Gaithersburg, MD, NIST Special Publication 1018-5, 2007.

[3] V. Molkov, D. Makarov, and A. Grigorash, "Cellular Structure of Explosion Flames: Modeling and Large-Eddy Simulation," *Combustion Science and Technology,* vol. 176, pp. 851-865, 2004.

[4] V. Molkov, D. Makarov, and H. Schneider, "LES Modelling of an Unconfined Large-Scale Hydrogen-Air Deflagration," *Journal of Physics D: Applied Physics,* vol. 39, pp. 4366-4376, 2006.

[5] V. Molkov, D. Makarov, F. Verbecke, Z. Mansurov, and M. Zhumabaev, "LES Model of Vented Explosion: Hydrogen-Air Mixtures," in *5th International Seminar on Fire and Explosion Hazards*, Edinburgh, 2007.

[6] D. Veynante and L. Vervisch, "Turbulent Combustion Modeling," *Progress in Energy and Combustion Science,* vol. 28, pp. 193-266, 2002.

[7] R. Knikker, D. Veynante, and C. Meneveau, "*A Priori* Testing of a Similarity Model for Large Eddy Simulations of Turbulent Premixed Combustion," *Proceedings of the Combustion Institute,* vol. 29, pp. 2105-2111, 2002.

[8] M. Boger, D. Veynante, H. Boughanem, and A. Trouvé, "Direct Numerical Simulation Analysis of Flame Surface Density Concept for Large Eddy Simulation of Turbulent Premixed Combustion," *Proceedings of the Combustion Institute,* vol. 27, pp. 917-925, 1998.

[9] G. M. Makhviladze, J. P. Roberts, and S. E. Yakush, "Modelling the Fireballs from Methane Releases," in *Proceedings of the Fifth International Symposium*: International Association for Fire Safety Science, 1997, pp. 213-224.

[10] G. M. Makhviladze, J. P. Roberts, and S. E. Yakush, "Numerical Modelling of Fireballs from Vertical Releases of Fuel Gases," *Combustion Science and Technology,* vol. 132, pp. 199-223, 1998.

[11] G. M. Makhviladze, J. P. Roberts, and S. E. Yakush, "Combustion of Two-Phase Hydrocarbon Fuel Clouds Released into the Atmosphere," *Combustion and Flame,* vol. 118, pp. 583-605, 1999.

[12] G. M. Makhviladze, J. P. Roberts, and S. E. Yakush, "Modelling and Scaling of Fireballs from Single -and Two-Phase Hydrocarbon Releases," in *Proceedings of the Sixth International Symposum*: International Association for Fire Safety Science, 2000, pp. 1125-1136.

[13] G. M. Makhviladze and S. E. Yakush, "Modelling of Fires Following Bursts of Pressurized Fuel Tanks," in *Proceedings of the Seventh International Symposium*: International Association for Fire Safety Science, 2003, pp. 643-654.

[14] P. Domingo, L. Vervisch, and K. Bray, "Partially Premixed Flamelets in LES of Nonpremixed Turbulent Combustion," *Combustion Theory and Modelling,* vol. 6, pp. 529-551, 2002.

[15] C. M. Müller, H. Breitbach, and N. Peters, "Partially Premixed Turbulent Flame Propagation in Jet Flames," *Proceedings of the Combustion Institute,* vol. 25, pp. 1099-1106, 1994.

[16] J. Wiley and A. Trouvé, "Large Eddy Simulation of Ignition and Transient Combustion in Fuel Vapor Clouds," in *Fifth International Seminar on Fire and Explosion Hazards* Edinburgh, 2007.

[17] J. Williamson, J. McGill, and A. Trouvé, "Large Eddy Simulation Modeling of Turbulent Deflagrations," in *Proceedings of the Eighth International Symposium*: International Association for Fire Safety Science, 2005, pp. 1375-1388.

[18] J. Williamson, J. McGill, and A. Trouvé, "A Filtered Progress Variable Approach to Model Turbulent Premixed Combustion in FDS," in *Congress on Computational Simulation Models in Fire Engineering and Research*, Univ. Cantabria, Santander, Spain, 2004, pp. 7-16.

[19] K. McGrattan, J. Floyd, G. Forney, H. Baum, and S. Hostikka, "Improved Radiation and Combustion Routines for a Large Eddy Simulation Fire Model," in *Proceedings of the Seventh International Symposium*: International Association for Fire Safety Science, 2003, pp. 827-838.

[20] T. Poinsot and D. Veynante, *Theoretical and Numerical Combustion*, 2nd ed.: Edwards, 2004.

[21] F. Williams, *Combustion Theory*, 2nd ed.: Benjamin/Cummings, 1985.

[22] E. R. Hawkes and R. S. Cant, "A Flame Surface Density Approach to Large-Eddy Simulation of Premixed Turbulent Combustion," *Proceedings of the Combustion Institute,* vol. 28, pp. 51-58, 2000.

[23] F. Charlette, A. Trouvé, M. Boger, and D. Veynante, "A Flame Surface Density Model for Large Eddy Simulations of Turbulent Premixed Combustion," in *Joint Meeting of the British, German, and French Sections of the Combustion Institute* Nancy, France: Combustion Institute, 1999.

[24] M. Boger and D. Veynante, "Large Eddy Simulation of a Turbulent Premixed V-Shaped Flame," in *Advances in Turbulence*, 8th ed, C. Dopazo, Ed. Barcelona: Cimne, 2000, pp. 449-452.

[25] M. Boger, "Modélisation de Sous-Maille pour la Simulation aux Grandes Echelles de la Combustion Turbulente Prémélangée." vol. Ph.D. Thesis: Ecole Centrale Paris, 2000.

[26] N. Peters, "Local Quenching Due to Flame Stretch and Non-Premixed Turbulent Combustion," *Combustion Science and Technology,* vol. 30, pp. 1-17, 1983.

[27] C. D. Pierce and P. Moin, "A Dynamic Model for Subgrid-Scale Variance and Dissipation Rate of a Conserved Scalar," *Physics of Fluids,* vol. 10, pp. 3041-3044, 1998.

[28] Z. Hu, G. Panafieu, J. Stauder, and A. Trouvé, "A Presumed Pdf Approach to Model Turbulent Non-Premixed Combustion in FDS," in *Congress on Computational Simulation Models in Fire Engineering and Research*, Univ. Cantabria, Santander, Spain, 2004, pp. 281-295.

[29] B. F. Magnussen and B. H. Hjertager, "On Mathematical Modeling of Turbulent Combustion with Special Emphasis on Soot Formation and Combustion," *Proceedings of the Combustion Institute,* vol. 16, pp. 719-729, 1976.

[30] I. Yamaoka and H. Tsuji, "The Structure of Rich Fuel-Air Flames in the Forward Stagnation Region of a Porous Cylinder," *Proceedings of the Combustion Institute,* vol. 15, pp. 637-644, 1974.

[31] I. Yamaoka and H. Tsuji, "Structure Analysis of Rich Fuel-Air Flames in the Forward Stagnation Region of a Porous Cylinder," *Proceedings of the Combustion Institute,* vol. 16, pp. 1145-1154, 1976.

[32] I. Yamaoka and H. Tsuji, "An Experimental Study of Flammability Limits Using Counterflow Flames," *Proceedings of the Combustion Institute,* vol. 17, pp. 843-855, 1978.

[33] C. K. Law, D. L. Zhu, T. X. Li, S. H. Chung, and J. S. Kim, "On the Structure and Extinction Dynamics of Partially-Premixed Flames: Theory and Experiment," *Combustion Science and Technology,* vol. 64, pp. 199-232, 1989.

[34] Z. Shu, C. W. Choi, S. K. Aggarwal, V. R. Katta, and I. K. Puri, "Gravity Effects on Steady Two-Dimensional Partially Premixed Methane-Air Flames," *Combustion and Flame,* vol. 118, pp. 91-107, 1999.

[35] C. W. Choi and I. K. Puri, "Flame Stretch Effects on Partially Premixed Flames," *Combustion and Flame,* vol. 123, pp. 119-139, 2000.

[36] J. Wiley and A. Trouvé, "Large Eddy Simulations of Flash Fires Following Ignition of a Fuel Vapor Cloud," in *Fifth US Combustion Meeting,* San Diego, CA, 2007.